An RXLR effector targets ER-Golgi interface to induce ER stress and necrotic cell death

Jihyun Kim[1,2], Jesse Kaleku[3], Haeun Kim[1,2], Minji Kang[1,2], Hui Jeong Kang[1,2], Cecile Segonzac[1], Jongchan Woo[3], Eunsook Park[3*], Doil Choi[1,2*]

[1] Horticultural Biotechnology, Department of Agriculture, Forestry and Bioresources, Plant Genomics and Breeding Institute, Seoul National University, Seoul, 08826, Republic of Korea

[2] Plant Immunity Research Center, Seoul National University, Seoul, 08826, Republic of Korea

[3] Department of Molecular Biology, University of Wyoming, WY USA

Running title: RXLR effector in ER stress-triggered necrotic cell death

***Correspondence**: Eunsook Park (epark4@uwyo.edu), Doil Choi (doil@snu.ac.kr)

Abstract

To achieve successful colonization, the pathogen secretes hundreds of effectors into host cells to manipulate the host's immune response. Despite numerous studies, the molecular mechanisms underlying effector-induced necrotic cell death remain elusive. In this study, we identified a novel virulent RXLR effector named Pc12 from *P. capsici.* Pc12 induces necrosis by triggering a distinct ER stress response through its interaction with Rab13-2. Unlike conventional hypersensitive response cell death associated with effector-triggered immunity, Pc12-induced cell death does not coincide with defense gene expression. Instead, it induces the relocalization of ER-resident proteins and confines secretory proteins within the ER. Pc12 interacts with Rab13-2, exhibiting a specific affinity for the active form of Rab13-2. Thus, it mimics the conformation of the inactive state of Rab13-2, subsequently recruiting the Rab-escort protein (REP). This process results in disruptions in vesicle formation within the ER-Golgi trafficking pathway. Furthermore, the substitution of a single amino acid of Rab13-2 structurally predicted to be crucial for the Pc12 interaction decreased the interaction with Pc12 while maintaining the interaction with REP and PRA1. These findings offer valuable insights into the ER stress-triggered cell death as well as a potential strategy for enhancing resistance against pathogens.

Keywords:

Phytophthora capsici, RXLR effector, Necrotic cell death, Rab Small GTPase, ER stress, Vesicle trafficking

Introduction

P. capsici is an oomycete pathogen causing blight disease in economically important crops, including *Cucurbitaceae*, *Solanaceae* and *Fabaceae* (Kamoun et al. 2015; Parada-Rojas et al. 2021; Quesada-Ocampo et al. 2023). *P. capsici* can inflict up to 100% crop damage in fields upon successful plant infection. This is attributed to its rapid proliferation under various environmental conditions, robust persistence in the soil over five years, and high genetic variability, leading to its classification as the fifth most destructive oomycete worldwide (Kamoun et al. 2015; Quesada-Ocampo et al. 2023). *Phytophthora* species secrete an arsenal of RXLR effector proteins to infect host plants. RXLR effectors feature a highly conserved Arg-X-Leu-Arg (RXLR) motif, which is essential for their transport into host cells (Whisson et al. 2007; Wawra et al. 2017). They play a significant role in facilitating the successful establishment of the pathogen by disrupting plant physiology and defense responses (Whisson et al. 2007; Fan et al. 2018; Boevink et al. 2020). Therefore, a comprehensive understanding of the role of RXLR effectors is important for devising strategies to manage plant diseases effectively.

The endoplasmic reticulum (ER) functions as a cellular factory responsible for protein synthesis, proper protein folding, and the export of proteins to subcellular organelles. These sequential processes must be balanced to maintain cellular homeostasis under environmental conditions (Cao and Kaufman 2012; Angelos et al. 2017; Adams et al. 2019). However, when an imbalance occurs, resulting in the accumulation of misfolded proteins known as ER stress, eukaryotic cells initiate the unfolded protein response (UPR). The UPR involves the translocation of two key transcription factors (bZIP28/60) from the ER membrane to the nucleus through maturation processes. This translocation improves UPR chaperone transcription and production, enhancing protein folding capacity in cells (Cao and Kaufman 2012; Angelos et al. 2017; Adams et al. 2019). However, if plants are subjected to severe or chronic stress, it can further lead to unresolved ER stress-induced programmed cell death (PCD) as a survival mechanism (Yang et al. 2014; Liu and Howell, 2016; Yang et al. 2021; Simoni et al. 2022).

Rab is a superfamily of small GTPases that plays a crucial role in intracellular vesicle trafficking, an essential process for the transfer of proteins, lipids, and other cellular materials between different membrane compartments within eukaryotic cells (Nielsen et al. 2008;

Stenmark et al. 2009; Pylypenko et al. 2018; Gray et al. 2020). Within a species, Rab proteins exist in multiple isoforms, each defining membrane identity and mediating vesicle trafficking to distinct subcellular compartments. Rab proteins function in the formation and guide of vesicles by acting as molecular switches, cycling between an active GTP-bound form and an inactive GDP-bound form (Nielsen et al. 2008; Stenmark et al. 2009; Pylypenko et al. 2018; Gray et al. 2020). Dysfunctional Rab proteins in vesicle trafficking can result in ER stress due to improper protein compartmentation. Several effectors of various pathogens are known to suppress antimicrobial protein secretion (PR1 and PDF1.2) or subvert vesicle movement toward the pathogen's focal area by targeting Rab proteins (Tomczynska et al. 2018; Pandey et al. 2021; Li et al. 2022). However, it remains elusive how the RXLR effector leads to ER stress-induced cell death by disrupting Rab proteins in vesicle trafficking.

In this study, we report a virulent RXLR effector Pc12 from *P. capsici*, triggering necrotic cell death in plants of the *Solanaceae*. Transient overexpression and host-induced gene silencing (HIGS) of *Pc12* in plants significantly affected the pathogenicity of *P. capsici*. Pc12 induced ER stress, resulting in distinct expression patterns of UPR genes and altering the location of ER-resident proteins and the secretory pathway. Notably, in the presence of Pc12, an active conformation of Rab13-2 attracted the Rab-escort protein (REP), enhancing its interaction. We have also identified a crucial residue in Rab13-2 to avoid Pc12 interference while retaining its original function in interacting with REP and PRA1. Consequently, this study provides valuable insights suggesting that modifying Rab13-2 to evade effector targeting could be a promising strategy for combating the pathogen infection while preserving its essential functions.

Results

Pc12 induces cell death independently of the plant defense mechanism in *Solanaceae* plants.

Among the previously selected RXLR effector candidates (Seo et al. 2023), Pc12 exhibited a strong induction of cell death in *N. benthamiana*. Interestingly, Pc12 consistently induces cell death in other *Solanaceae* species when transiently expressed in *N. tabacum, C. annuum,* and *S. lycopersicum* (Figure 1A), suggesting that Pc12-induced cell death is more pronounced within the *Solanaceae* family. To determine whether the observed cell death induced by Pc12 resulted from an NLR-mediated hypersensitive response (HR), we investigated Pc12-mediated

cell death in *N. benthamiana* plants with individual silencing of NLR-downstream signaling factors, including *SGT1, EDS1, ADR1/NRG1,* and *NRC234* (Botër et al. 2007; Dongus and Parker, 2021; Wu et al. 2017). Interestingly, Pc12-induced cell death remained unaffected by the silencing of downstream signaling components (Figure 1B-D), suggesting that Pc12 induces cell death through mechanisms that are distinct from those typically associated with NLR-mediated effector-triggered immunity (ETI). To further validate whether the cell death induced by Pc12 is independent of HR cell death, we compared the expression of defense-related genes during Pc12 expression in contrast to the expression of a bacterial effector derived from *Xanthomonas spp.,* XopQ. XopQ is known to interact with the resistance protein Roq1 in *N. benthamiana*, resulting in a mild chlorotic phenotype (Schultink et al. 2017). Transcription of defense-related genes, including *PR1, RbohB,* and *WRKY8*, exhibited significant upregulation upon transient overexpression of XopQ. In contrast, the expression of Pc12 did not notably induce the expression of defense-related genes (Figure 1E), which supports the idea that the cell death triggered by Pc12 may activate a distinct molecular pathway compared to HR elicited by the ETI.

Pc12 functions as a virulence effector, enhancing the pathogenicity of *P. capsici*.

Pc12 expression is elevated during the biotrophic phase of *P. capsici* (Supplemental Figure 1). Although Pc12 displays the canonical structure of an RXLR effector, it remains uncertain whether Pc12 is a virulent effector for *P. capsici* colonization. To assess the impact of Pc12 on the virulence of *P. capsici*, the pathogen was inoculated in plants expressing Pc12 under the control of an ethanol-inducible promoter without ethanol treatment (Figure 2A). Leaky expression of Pc12 driven by the ethanol-inducible promoter (Lee et al. 2018) allows us to generate weak expression of Pc12 avoiding rapid cell death. The *Agrobacterium* carrying construct of RFP or RFP-Pc12 was infiltrated into *N. benthamiana*, followed by drop inoculation of *P. capsici* onto the leaves one day post infiltration. We observed a substantial increase in lesion size (Figure 2A) and *P. capsici* biomass (Figure 2B). Host-induced gene silencing (HIGS) is a method that initiates targeted gene suppression in the pathogen through the host's RNA interference (RNAi) machinery (Cheng et al. 2022). Consistently, the silencing of Pc12 by HIGS using TRV compromised the pathogenicity of *P. capsici* compared to the control (Figure 2C-D), which implies that Pc12 elevates *P. capsici* pathogenesis as a virulence

effector.

Pc12 expanded lineage-specifically in *P. capsici* and the C-terminal residue is crucial for inducing cell death.

To elucidate whether Pc12 functions as a single gene or as part of a gene family, we examined the copy number variation and sequence polymorphism of Pc12 homologs in *Phytophthora* spp. The sequence polymorphism of Pc12 was assessed through a BLAST search, encompassing genome sequences from *P. capsici* (ten strains; CPV-219/262/267/270/277/302, KPC-7, MY-1, and JHAI1-7) and four other *Phytophthora spp.* (*P. ramorum* Pr102, *P. sojae* P6497, *P. cinnamoni* CBS144.22, and *P. infestans* T30-4) retrieved from the public database. Analysis revealed that the *P. capsici* strains contain a notably higher number of Pc12 homologs in their genome compared to other *Phytophthora* pathogens (Supplemental Table 1, Reyes-Tena et al. 2019; NCBI reference sequence database (RefSeq)). To determine whether the Pc12 homologs of these *Phytophthora spp.* could induce cell death, three homologs of *P. capsici* LT1534 and one homolog each of *P. ramorum, P. sojae,* and *P. cinnamomi* were synthesized and transiently expressed in *N. benthamiana*. Interestingly, the cell death phenotype was exclusively observed with *P. capsici* homologs, except PHYCA22034 (Supplemental Figure 2). Although Pc12 and PHYCA22034 share 85% identity, substantial differences are found at the C-terminal end, suggesting that this difference could be responsible for their distinct abilities to induce cell death (green line in Figure 2E). To determine the importance of the C-terminus of Pc12 in triggering cell death, we generated a series of chimeric mutants modified amino acids at the C-terminus (Figure 2F). The substitution of amino acids from the 91st to 95th position of Pc12 in PHYCA22034 resulted in mild cell death, whereas the substitution of amino acids from the 89th to the 95th position fully restored cell death in *N. benthamiana* (Figure 2G). Consistently, a truncated Pc12 lacking the five amino acids at the C-terminus lost its ability to induce cell death (Pc12ΔC5 in Figure 2G). These results suggest that functional Pc12 has undergone a lineage-specific expansion within *P. capsici*, and the C-terminal sequence plays a pivotal role in triggering cell death in plants.

Pc12 interaction with Rab13-2 small GTPase via 5 amino acids at the C-terminus is essential for cell death.

Previously, one of Pc12 homologs was shown to induce cell death by its transient expression in *N. benthamiana* (Li et al. 2019) and, interestingly, this isoform also interacts with one of the Rab 13 protein (Rab 13-4) that colocalizes with the ER and nucleus (Li et al. 2022). To validate weather Pc12 interacts with Rab proteins, we performed immunoprecipitation and mass spectrometry (IP-MS) using Pc12 and Pc12ΔC5. The list of proteins exclusively interacting with Pc12 but not with Pc12ΔC5 includes a small GTPase Rab13-2 protein in the highest score of peptide-spectrum match (PSM) (Supplemental Table 2). We confirmed *in planta* interaction between Pc12 and Rab13-2 by a co-immunoprecipitation (co-IP) assay, while no such association was observed with Pc12ΔC5 (Figure 3A). Homologs of Pc12 that trigger cell death also presented interaction with Rab13-2 (Figure 3A). This implies that the interaction between Pc12 homologs that share a similar C-terminus with Rab13-2 is crucial for the induction of cell death. Rab small GTPase is a superfamily protein functionally conserved in eukaryotic cells (Nielsen et al. 2008, Pylypenko et al. 2018, Nielsen et al. 2020). Typically, the family comprises more than 60 isoforms that reside in specific membrane compartments generated during membrane trafficking in eukaryotic cells (Stenmark 2009, Pylypenko et al. 2018, Nielsen et al. 2020). In the *N. benthamiana* genome, the Rab protein family consists of 149 genes (Supplemental Figure 3). To explore the specificity of the interaction between Pc12 and Rab13-2, co-immunoprecipitation experiments were performed with Rab13-2 homologs. Pc12 was found to selectively bind to Rab13-3 and Rab13-4, which shared an amino acid sequence similarity of 98% and 91% with Rab13-2, respectively (Figure 3B). This suggests that Pc12 prefers to interact with specific Rab13-2 homologs. Rab proteins contain two loops in their globular region, which undergo allosteric conformational changes depending on whether Rab13-2 is bound to GTP or GDP. In the GTP-bound state, these loops draw closer, leading to a compact structure. On the contrary, Rab proteins bound to GDP exhibit a more relaxed structure (Gray et al. 2020). To ascertain the specific conformation of Rab13-2 targeted by Pc12, we generated mutants representing constitutively active (Rab 13-2^{Q74L}) or inactive form (Rab13-2^{S29N}) of Rab13-2. Co-IP assays demonstrated that Pc12 exclusively interacts with only the active form of Rab13-2 (Figure 3D). The direct interaction of Pc12 and Rab13-2 was further confirmed by a yeast-two-hybrid (Y2H) assay (Figure 3E). Supportively, no interaction is observed between Rab 13-2 and Pc12ΔC5, underscoring the importance of the C-terminus of Pc12 in facilitating the interaction of Pc12 and Rab13-2.

Pc12 might interfere with Rab 13-2 trafficking at the ER-Golgi interface

Rab proteins are known for their distinct localization within the plant endomembrane network (Stenmark 2009; Nielsen et al. 2020). The hypervariable C-terminal region of Rab proteins contributes to the specificity of membrane delivery for certain Rab proteins (Figueroa et al. 2001; Pylypenko et al. 2018). Previously, a Pc12 isoform was identified to interact with an isoform in the Rab 13 subfamily (Rab13-4, in this study) and both reside on the ER (Li et al. 2022). To gain insight into the localization of Pc12 within host cells, we transiently expressed EGFP-Pc12 and EGFP- Pc12ΔC5 (excluding the signal peptide and RXLR-EER motifs). Due to the rapid induction of cell death by Pc12, cytosolic Pc12 expression was observed in the early time point after the induction of gene expression by ethanol to determine its subcellular location (Figure 4A). Interestingly, unlike the previously studied isoform, the Pc12 proteins are defused in the cytoplasm with preferential accumulation closer to the ER and Golgi (left panels of Figure 4A). Pc12ΔC5 localization is similar to Pc12. However, Rab13-2 localized in the cytoplasm at the peri-ER and Golgi (right panels of Figure 4A). Notably, while the potential constitutive inactive form Rab13-2 ^{S29N} was frequently observed at the Golgi apparatus, a constitutive active form Rab 13-2^{Q74L} did not show a Golgi localization (right panels of Figure 4A), which showed a similar localization pattern to Pc12.

Pc12 enhances the formation of the Rab13-2 and REP complex, not PRA1, by mimicking the inactive conformation of Rab13-2 to attract REP.

Rab proteins are involved in vesicle budding, transport, and fusion processes by interacting with or recruiting other proteins (Stenmark 2009; Pylypenko et al. 2018; Nielsen et al. 2020). In the case of Rab13-2, potential interactors were identified using the STRING database (Supplemental Table 3). Among the interactors, the Rab escort protein (REP) and the prenylated Rab acceptor protein 1 (PRA1) were found to interact with Rab13-2 through co-IP screening. REP functions as a chaperone, facilitating the prenylation process of Rab, and a carrier, guiding Rab to its destination membrane (Guo et al. 2008). PRA1 acts as a receptor for prenylated Rab proteins, promoting their binding to membranes (Figueroa et al. 2001). We hypothesized that Pc12 might influence the interaction between Rab13-2 and its interactors, REP or PRA1. To confirm the impact of Pc12 on these interactions, we conducted an

immunoprecipitation experiment. Rab13-2 and its interactors were constitutively expressed in a plant, while Pc12 was induced by ethanol treatment at 1 dpi (day post-infiltration), ensuring that Pc12's action did not affect the accumulation of newly synthesized proteins. The results showed that Pc12 did not form a complex with Rab13-2 in the presence of PRA1, indicating that PRA1 prevents the association between Pc12 and Rab13-2 (Figure 4C). Intriguingly, the interaction between Rab13-2 and REP was strengthened with the expression of Pc12 (red asterisk in Figure 4C). This implies that Pc12 plays a regulatory role in the association between Rab13-2 and REP, potentially influencing their cellular functions and signaling pathways. Pc12 preferentially binds to the active form of Rab13-2 (Rab 13-2^{Q74L}, Figure 3). However, REP is known to interact predominantly with the inactive form (Stenmark 2009, Supplemental Figure 5). Therefore, we hypothesized that Pc12 binds to the active form of Rab13-2, which mimics the conformation of inactive Rab13-2. Consequently, Pc12 can contribute to REP recruitment to Rab13-2 by emulating its allosteric conformation. To validate this hypothesis, we performed a co-IP with Pc12, Rab13-2^{Q74L}, Rab13-2^{S29N}, and REP, respectively following the same experimental strategy. Interestingly, REP demonstrated a significant association with Rab13-2^{Q74L} in the presence of Pc12, compared to the control RFP (red asterisk in Figure 4D). This finding suggests that Pc12 binds to the active state of Rab13-2, facilitating the recruitment of REP. This recruitment can lead to either disassociation of active Rab13-2 from the membrane or aggregation of the complex on the membrane, ultimately resulting in the disruption of vesicle trafficking.

In this notion, we examined whether the localization of Rab13-2 might alter upon coexpression of Pc12. Remarkably, larger punctate localizations of GFP-Rab 13-2^{Q74L} were frequently observed under the expression of Pc12 (yellow arrows, Figure 4E), while they were not typically observed with RFP or Pc12ΔC5. Furthermore, the Golgi association of GFP-Rab13-2^{S29N} was disrupted under the Pc12 expression (white arrowheads, Figure 4E). The results suggest that Pc12 changes the property of Rab 13-2^{Q74L} to mimic the status of Rab13-2^{S29N}, recruiting REP effectively and, consequently, localizing at Golgi.

Pc12 alters the integrity of the ER and elicits ER stress that causes necrotic cell death.

The altered localization of Rab 13-2^{Q74L} with Pc12 indicates that the rapid dissociation of active Rab proteins and their return to the ER periphery might be interrupted under Pc12 expression.

To test whether the ER retention pathway is affected by Pc12, EGFP-Pc12 was expressed in a transgenic *N. benthamiana* plants expressing RFP fused with ER retention signal peptides (HDEL). RFP-HDEL typically displays a reticular ER morphology when observed under a microscope. This is because newly synthesized proteins containing HDEL undergo initial synthesis in the ER lumen, followed by transport to the Golgi apparatus, and subsequent return to the ER through signal recognition (Alvim et al. 2023). Under the same conditions that we observed cytosolic Pc12 (Figure 4A), we could observe that some cells showed a peculiar puncta localization of RFP-HDEL in the cell (middle panel of Figure 5A), while the reticular morphology of ER visualized by RFP-HDEL is unchanged under the expression of EGFP or EGFP-Pc12ΔC5 (Figure 5A). The punctate pattern of RFP-HDEL induced by Pc12 suggests that it may be caused by interference with the retrieval of RFP-HDEL proteins from Golgi to the ER. Interestingly, an apoplast makers of moxVenus fluorescent proteins, fused to an apoplastic signal peptide at the N-terminus and a C-terminal transmembrane domain, anchor the fluorescence protein outside the plasma membrane (ApoSP-moxVenus-TM, Balleza et al. 2017) are trapped in the ER in the presence of RFP-Pc12 (Figure 5B), evidently suggesting that Pc12 disrupts vesicle trafficking at the ER-Golgi interface, leading to alteration of marker localizations.

The mutualistic fungus *Piriformospora indica* was reported to induce ER-stress triggered cell death when it colonizes *Arabidopsis* roots (Qiang et al. 2012). Interestingly, the altered ER morphology by *P. indica* infection is similar to that of the expression of Pc12 (Qiang et al. 2012, Figure 5A). Therefore, we compared the responses triggered by Pc12 and Tunicamycin, a well-known inducer of ER stress. These responses include an accumulation of ER-chaperon binding immunoglobulin protein (BiP) and the transcription of unfolded protein response (UPR) genes (Cao and Kaufman 2012; Angelos et al. 2017; Adams et al. 2019; Yang et al. 2014). To regulate the expression of Pc12 and a control, we cloned Pc12 fused with RFP (RFP-Pc12) and RFP alone into an expression vector controlled by an ethanol-inducible promoter. Subsequent treatment with 10% ethanol in plants led to the progressive accumulation of both RFP-Pc12 and RFP proteins over time. As hypothesized, RFP-Pc12 induced gradual accumulation of BiP, similar to the effects of Tunicamycin treatment, over time (Figure 5C). To evaluate the expression of UPR-related genes, samples were collected at 0 and 12 hour post-treatment. Tunicamycin treatment upregulated transcripts for both ER stress-related transcription factors

(*bZIP28* and *bZIP60*) and ER chaperons (BiP-like protein *BLP4* and calreticulin *CRT1*). However, the expression of Pc12 did not exhibit a similar upregulation pattern in ER chaperone transcripts. Instead, Pc12 induced an increase in the expression of transcription factors (Figure 5D). These findings suggest that Pc12 induces a distinct form of ER stress differnt from the effects of Tunicamycin.

A specific residue of Rab13-2 is crucial for its interaction with Pc12 and its mutation evading the targeting by Pc12 affect to the virulence of *P. capsici*.

The failure of effectors to suppress plant immunity by manipulating the function of host targets is deemed a contributing factor to nonhost resistance (NHR) (McLellan et al. 2022). Thus, breaking down the interaction between Pc12 and Rab13-2 might achieve disease resistance. To obtain a better estimate of the biochemical property of the Pc12 and Rab13-2 interaction, we used the AlphaFold2 program (Jumper et al. 2021) to identify a pivotal residue on Rab13-2 that interacts with the C-terminal AHQMG residues of Pc12. Rab13-2 was predicted to have a globular structure, whereas Pc12 displayed a stack of three parallel α-helices connected by a short helical inker (Figure 6A). A docking model proposed that the three-parallel α-helices of Pc12 interacted with the globular region of Rab13-2 (Figure 6A). Notably, L90, A91, and M94 at the C-terminus of Pc12 were predicted to engage with threonine at the 47th position of Rab13-2 (Figure 6B). Remarkably, replacement of threonine with alanine (Rab13-2^{T47A}) abolished the Rab13-2 interaction with Pc12 (Figure 6C), without compromising its ability to bind REP and PRA1(Figure 6D-E).

These results are significant in envisioning the potential of Rab proteins as a target to engineer resistant plants to *P. capsici*. To evaluate the applicability of the Rab13-2^{T47A} mutation for resistance to *P. capsici*, *N. benthamiana* plants expressing Rab13-2^{T47A} were inoculated with *P. capsici*. At 72 hpi, as the disease progressed, the lesion size with the expression of Rab13-2^{T47A} was significantly reduced compared to those with the expression of Rab13-2 (Figure 6F). Considering the impact of endogenous Rab13-2 might diminish the effect of the expression of Rab13-2^{T47A}, this result is significant to imply that Pc12 is a key player in determining the necrotrophic phase, and Rab13-2^{T47A} can serve as a contributing factor to delay the onset of the necrotrophic disease progression.

Discussion

Pc12 serves as a transition effector, orchestrating the transition from the biotrophic to the necrotrophic life cycle of *P. capsici*.

P. capsici is classified as a hemibiotrophic pathogen, marked by a biphasic life cycle. It commences with a biotrophic phase that strategically established itself within host plants. Subsequently, it progresses to a necrotrophic phase, aiming to extract nutrients from deceased cells and releasing spores for subsequent dissemination. (Kamoun et al. 2015; Parada-Rojas et al. 2021; Quesada-Ocampo et al. 2023). Although researchers have uncovered the roles of RXLR effectors in augmenting susceptibility by interfering with host cell physiology or triggering defense responses through interactions with R proteins during the biotrophic phase, our understanding of how these effectors induce necrosis in host cells remains quite limited. Recently, a case of necrosis in which a *P. infestans* RXLR effector was reported to induce nucleolar inflammation and impede pre-rRNA 25S processing, leading to necrosis through disruption of protein translation (Lee et al. 2023). In this study, the RXLR effector Pc12 was identified as a critical factor for necrosis causing severe ER stress by obstructing Rab13-2 recycling in vesicle trafficking. Furthermore, evasion of Pc12 targeting by Rab13-2^{T47A} led to a reduction in necrotrophic lesion size, highlighting that Pc12-induced necrosis contributes to the necrotrophic life cycle of the pathogen. Interestingly, Pc12 expression was highly upregulated at 6 hpi, while the transcripts of NPP1, a necrotrophic marker, gradually increased at 12 hpi (Supplemental Figure 1). This raises the question of why the transcription of Pc12 increased early in infection despite its role in inducing necrosis. In the experiment using the ethanol-inducible promoter, the accumulation of the Pc12 protein was detected at 9 hpt and cell death was observed prior to 24 hpt to the naked eye, following ethanol treatment (Figure 5C). Given the time delay from gene transcription to necrosis induction, it could be inferred that Pc12-induced necrosis serves as an initiator for entering the necrotrophic phase.

The emergence of Pc12 benefits *P. capsici* by broadening its host range and promoting survival.

Within the *Phytophthora* genus, only *P. capsici* possesses multiple copies of at least 8 homologs of Pc12 with the potential to induce necrosis. In contrast, *P. ramorum*, *P. cinnamoni*, and *P. sojae* lack this specific feature. (Supplemental Table 1, Supplemental Figure 2). The relatively

recent emergence of *P. capsici*, along with its closer relationship with *P. infestans* compared to other species (Lamour et al. 2012), implies that the Pc12 family likely evolved subsequent to the evolution of the *P. capsici* species and lineage-specifically expanded in the species. Given the distinctive characteristics of *P. capsici*, the emergence of Pc12 has led to two positive outcomes. First, Pc12 disrupts vesicle trafficking in the basal physiology of plants, enabling *P. capsici* to infect a wider range of hosts compared to *P. infestans* and *P. sojae*. Second, Pc12 induces necrosis rapidly, prompting *P. capsici* to shorten its biotrophic phase to approximately 30 hpi, in contrast to *P. infestans* and *P. sojae* (2 days). This acceleration could assist *P. capsici* in establishing itself sufficiently before the onset of the host's defense response, thereby enabling the pathogen to evade the early immune responses. With these advantages conferred by Pc12, *P. capsici* may have the potential to cause extensive damage to a broad spectrum of hosts, often leading to crop losses of up to 100%.

Pc12 disrupts the Rab13-2 cycle by augmenting the affinity of REP to the active structure of Rab13-2.

Numerous studies have reported that pathogenic effectors target vesicle-related proteins to hinder the secretion of defense-related proteins or to subvert autophagy to obtain nutrients for pathogen nourishment (Gu et al. 2017; Pandey et al. 2021; Petre et al. 2021; Yuen et al. 2023). In our research, we have identified that Pc12 targets Rab13-2, disrupting vesicle trafficking between the ER and Golgi. This disruption results in the accumulation of apoplastic proteins in the ER lumen and even the nucleus (Figure 5). In a similar manner, the viral replicase p27 of *Red clover necrotic mosaic virus* (RCNMV) inhibits vesicle trafficking between the ER and Golgi by relocating Arf1 for COPI and Sar1 for COPII to the ER, resulting in the accumulation of secretory proteins within the ER (Hyodo et al. 2013; Hyodo et al. 2014). Furthermore, we have discovered a novel strategy for the RXLR effector Pc12. It mimics the inactive conformation of Rab13-2 by binding to the active structure of Rab13-2, thereby enhancing the affinity of REP for the active form of Rab13-2 (Figure 4, 7). This strategy is similar to Brefeldin A, a fungal toxin that enhances the affinity of GEF to bind to GDP-bound Arf1, ultimately disrupting the cycle of Arf1 between GDP and GTP (Niu et al. 2005). Given the objectives shared with a viral protein and a fungal toxin, Pc12 significantly contributes to the pathogenicity of the pathogen.

Necrosis caused by Pc12 results from a distinct form of severe ER stress characterized by hyper-accumulation of proteins.

Both animals and plants possess evolutionarily conserved ER stress responses to a variety of stimuli (Oakes et al. 2015; Angelos et al. 2017). When ER dysfunctions become excessive or prolonged, cells initiate death signaling, akin to a survival strategy in multicellular organisms, aimed at eliminating dysfunctional cells (Oakes et al. 2015; Simoni et al. 2022). In animals, ER stress-induced cell death has been extensively studied, particularly in the context of diseases such as Alzheimer's and Parkinson's disease (Oakes et al. 2015). However, our understanding of ER stress-induced cell death in plants is still evolving, with some aspects yet to be fully elucidated. Pc12-induced inhibition of Rab13-2 recycling in vesicle trafficking leads to severe ER stress, ultimately culminating in necrosis. According to Yang et al. 2014, the transcription factor NAC089, transcribed by bZIP28/60, plays a pivotal role in controlling ER-stress-induced programmed cell death in plants, triggering the expression of PCD-related genes (NAC094, MC5, and BAG6) (Yang et al. 2014). Notably, Pc12 induces a substantial upregulation of bZIP28/60, but it does not lead to a commensurate increase in the expression of bZIP28/60-downsteam pathway genes (UPR-related genes, Figure 5D) and PCD-related genes (not data shown). When coupled with Pc12-induced disruption of vesicle trafficking between the ER and the Golgi, this implies that Pc12 hinders the relocation of bZIP28 to the Golgi and prevents the splicing of bZIP60, unless signaling of unresolved ER stress occurs. Consequently, this leads to suppression of genes regulated by bZIP28/60 (Figure 7). Furthermore, Ko et al. (2023) recently reported that ABI5 activates the transcription of bZIP60 under ER stress, suggesting the interpretation that Pc12 induces the upregulation of bZIP28/60 irrespective of bZIP28/60 translocation to the nucleus (Ko et al. 2023). However, the movement of ABI5 under ER stress remains unknown. Taken together, the failure to alleviate ER stress by Pc12 leads to an excessive accumulation of proteins in the ER, effectively acting as a cellular "time bomb" (Figure 7).

The point mutation of Rab13-2 has a potential to manipulate plant resistance against *P. capsici*.

The underlying molecular mechanism of nonhost resistance is believed to arise from 1)

411 preexisting barriers preventing pathogen establishment, 2) the detection of pathogen effector
412 proteins triggering robust immunity, and 3) the incapacity of pathogen effectors to suppress
413 immunity triggered by molecular patterns (McLellan et al. 2022). The inability of effectors to
414 manipulate host targets for pathogen colonization results in a hostile environment, leading to
415 the pathogen's failure to adapt to the host. This importantly implies that the evasion strategy
416 against effectors targeting, acting like an orchestra, results in robust resistance, enabling the
417 conversion from host to nonhost plants. We identified the specific residue in Rab13-2 that
418 avoids Pc12 targeting through AF2. The mutant of this residue resulted in a reduction in the
419 pathogenicity of *P. capsici*. This study provides insight into the idea that host plants can develop
420 resistance against *P. capsici* through the synergistic effects of various mutations evading other
421 effectors, collectively contributing to susceptibility.
422
423 **Materials and methods**
424 **Plant materials and growth conditions**
425 *N. benthamiana, N. tabacum* cv. Samsun, and *Solanum lycopersicum* cv. Heinz seeds were
426 directly sown into damp horticultural bed soil (Biogreen, Seoul, Korea) and cultivated within
427 a walk-in chamber at 22-24℃ under a 16h/8h (day/night) cycle. *Capsicum annuum* cv. ECW
428 seeds were sterilized for 1 min in a 0.1% sodium hypochlorite solution and germinated in
429 darkness at 30℃ for 7 days. Following this, the pepper seedlings were transplanted into soil
430 and grown within the same chamber. For virus-induced gene-silencing assays, 3-week-old *N.*
431 *benthamiana* were utilized. Transgenic *N. benthamiana* plants expressing RFP fused to HDEL
432 (ER marker, Nelson *et al*. 2007) was used in this study. Plants were grown at 22-24°C for 4-5
433 weeks prior to the corresponding experiments.
434
435 ***P. capsici* culture condition and inoculation assays**
436 *P. capsici* strain 40476 was cultured on V8 agar medium for 7 days at 23℃ in darkness. The
437 mycelia were scraped and then incubated under light for 12 hours. To induce the release of
438 zoospores, sporangia were harvested and placed in distilled water, incubating at 4℃ for 30
439 minutes, followed by 23℃ for 30 minutes. A total of 500 zoospores were inoculated on the
440 detached *N. benthamiana* leaves through droplets. The leaves were placed at 25℃ for 2 days
441 under deem light. The lesion areas were measured at 2 dpi.

442

443 **Constructs and markers preparation**

444 RXLR effector and their mutants were amplified, incorporating an N-terminal 3xHA epitope
445 excluding signal peptide and RXLR-EER motifs. Rab proteins and REP or PRA were amplified
446 with N-terminal GFP and 3xFLAG, respectively, employing the overlap PCR method (Kim et
447 al. 2017). GOIs were inserted into pCambia2300-LIC vector using the ligation-independent
448 cloning method (Oh et al. 2010). RFP and RFP-Pc12 were amplified with the attB site to insert
449 into ethanol-inducible expression vector using Gateway cloning (Invitrogen, USA). The primer
450 sequence used for construction are presented in Supplementary Table 3. mCherry targeted to
451 Golgi generated previously was used for Golgi marker (Addgene ID 97401, Park et al. 2017).
452 The membrane bound apoplastic marker constructs were generated by inserting a signal peptide
453 of *At*Chitinase in front of moxVenus yellow fluorescence protein sequences and C-terminal 26
454 amino acids of transmembrane domain at the end (Baleza et al. 2017, Berthold et al. 2019).
455 Plant expression constructs of Rab variants and apoplastic side membrane marker were
456 deposited to the Addgene (Rab13-2, ID:213473; Rab 13-2^{Q74L}, ID:213474; Rab13-2^{S29N},
457 ID:213475; ApoSP-moxVenus-TM, ID: 213477) constructs are deposited in Addgene.

458

459 **Agroinfiltration and quantification of cell death assays**

460 *Agrobacterium tumefaciens* GV3101 strain or GV2260 containing the various constructs were
461 cultivated overnight at 28℃ in LB medium supplemented with appropriate antibiotics. The
462 cells were harvested through centrifugation and then resuspended in an infiltration buffer (10
463 mM $MgCl_2$, 10 mM MES (pH 5.6), and 200 µM Acetosyringone). Resuspensions were adjusted
464 to an optical density (OD600) of 0.1-0.3 and leaves of 4-week-plants were agroinfiltrated for
465 transient expression. To quantify the degree of cell death, *N. benthamiana* leaves were detached
466 and measured using chlorophyll fluorescence, employing the default *Fv/Fm* protocol from a
467 closed FluorCam (Photon Systems Instruments, Czech Republic). The quantification analysis
468 was conducted using the FluorCam 7.0 software. For ethanol-inducible constructs, 10% ethanol
469 was sprayed on both the adaxial and abaxial sides of the infiltrated leaves at 24 hpi.

470

471 **Virus-induced gene silencing in *N. benthamiana* and host-induced gene silencing in *P.***
472 ***capsici***

Virus-induced gene-silencing (VIGS) procedure was conducted described to the protocol described by Liu et al. (2002). *A. tumefaciens* suspensions containing pTRV1 and pTRV2 with *SGT1, EDS1, ADR1/NRG1,* and *NRC2/3/4* were mixed at a 1:1 ratio in infiltration buffer (10 mM MES, 10 mM $MgCl_2$, and 200 µM Acetosyringone, pH 5.6) to a final optical density (O.D.) at 600 nm of 1.5. This mixture was infiltrated into two leaves of 2-week-old *N. benthamiana* plants. All plants were grown within a walk-in chamber at 24°C under a 16h/8h (day/night) cycle. After 3 weeks, the upper leaves were utilized for further experiments assessing the efficiency of silencing. Host-induced gene silencing (HIGS) was conducted following the VIGS procedure. After 3 weeks, *P. capsici* strain 40476 was inoculated onto the detached upper leaves. After 6 hours, four leaf discs containing zoospores were collected to evaluate the silencing efficiency.

Extraction of DNA and RNA and gene expression analysis by qPCR

To assess the biomass of *P. capsici,* total genomic DNA was extracted from four leaf discs adjacent to the *P. capsici*-inoculated area using cetyltrimethylammonium bromide (CTAB) method. For gene expression analysis, total RNA was extracted from four leaf discs using TRIzol reagent (TR118, MRC, USA), and cDNA synthesis was conducted using Superscript II (18064014, Invitrogen, USA) following the manufacturer's instructions. Quantitative PCR (qPCR) and quantitative reverse-transcription PCR (qRT-PCR) was performed utilizing ExcelTaq™ 2X Q-PCR Master Mix (SYBR, ROX; TQ1110, SMOBIO, Taiwan) with a CFX96 Touch Real-Time PCR Detection System (Bio-Rad, USA). The expression of the PcActin gene was normalized to elongation factor-1a of *N. benthamiana* (NbEF-1a), and the transcript levels were normalized using the internal standard (NbEF-1a). The primer sequences used in this study are provided in Supplemental Table 4.

Yeast two hybrid assay

Pc12 and truncated Pc12 were cloned into pGBKT7 vector (Takara Bio, Japan), while Rab13-2 and Rab13-2 mutants were inserted into pGADT7 vector. The recombinant plasmids, pGBKT7 and pGADT7, were introduced into yeast strain Y2HGold and Y187, respectively. For yeast two hybrid assay, yeast mating was performed in yeast peptone dextrose adenine (YPDA) medium at 30°C overnight. The resulting colonies were recovered on a Synthetic

Defined medium lacking tryptophan and leucine (SD/-Lue-Trp), and the interactions were validated on SD medium lacking histidine, leucine, and tryptophan (SD/-Lue-Trp-His). The medium plates were incubated at 28°C and typically photographed in 5 days. For positive and negative controls, commercial yeast constructs were used: positive control (pGBKT7-p53/pGADT7-T) and negative control (pGBKT7-p53/pGADT7-Lam), both provided by Matchmaker™ Gold Yeast Two-Hybrid System (630489, Clontech, USA).

Co-immunoprecipitation, immunoblot assays, and IP-MS analysis

N. benthamiana leaves infiltrated with *Agrobacterium* were sampled at 24–30 hpi for co-IP or western blotting. Total protein was extracted using an extraction buffer (10% [v/v] glycerol, 25 mM Tris–HCl [pH 7.5], 1 mM EDTA, 150 mM NaCl, 1% [w/v] polyvinylpolypyrrolidone, and 1× protease inhibitor cocktail). The extracted proteins were immunoprecipitated with 10 ul of anti-HA magnetic beads (M180-10, MBL, Japan), anti-GFP agarose beads (D153-8, MBL, Japan), or anti-FLAG agarose beads (651502, BioLegend, USA) and incubated for 4 hours or overnight at 4°C. The beads were washed ten times with immunoprecipitation wash buffer (GTEN extraction buffer with 0.015% [v/v] Triton X-100) and resuspended in 10 µl SDS loading dye. Proteins were eluted from the beads by heating at 95°C for 5 min. For western blotting, the immunoprecipitated and input proteins were separated on SDS–PAGE gels and transferred onto PVDF membranes via a Trans-Blot Turbo Transfer System (Bio-Rad, USA). After blocking the membranes with a solution of 5% skim milk prepared in PBST with 0.1% Tween 20, they were incubated with HRP anti-RFP (1:12000, M204-7, MBL, Japan), HRP anti-GFP (1:12000, AB6663, Abcam, UK), HRP anti-HA (1:12000, AB173826, Abcam, UK), or HRP anti-FLAG (1:12000, A8592, Sigma, USA) antibodies at room temperature for 1 h. The membrane was washed twice with PBST for 10 min each before ECL (1705061, Bio-Rad, USA) detection was performed according to the manufacturer's instructions. For IP-Mass analysis, immunoprecipitated proteins were collected on SDS–PAGE gels and the samples were analyzed using High Resolution LC/MSMS spectrometer (Q Exactive, Thermo Scientific, USA) in NICEM (National Instrumentation Center for Environmental Management, College of Agriculture and Life Sciences, Seoul National University Seoul 151-742, Korea)

Confocal microscopy

For a confocal microscopy, 5 mm^2 *N. benthamiana* leaf discs of the infiltrated region were observed 36 hours post *Agrobacteria* infiltration. Images were acquired with an Olympus IX83spinning disk confocal microscope (yokogawa CSW-W1 SoRA) equipped with an ORCA-Fusion Digital CMOS camera under 60 X oil immersion objective (N.A., 1.3) by sequential detection of average of 76 Z stacks. For the laser scanning confocal microscopy, images were generated on a ZEISS LSM980 AiryScan super resolution microscope system using Axio observer Z1 inverted microscope with 40X/1.2 NA C-Apochromat water immersion objective using the 514nm and 561nm laser lines for moxVenus and RFP imaging respectively. 5% laser power was used for imaging moxVenus with excitation at 525nm and detection between 517-581nm: 8% laser power was used to detect RFP with excitation at 590nm and detection between 578-654nm. Images were processed using Fiji ImageJ (National Institutes of Health, Bethesda, Maryland, USA) from the maximum Z intensity projections of the confocal images. Fiji ImageJ was also used to generate the chromatograms from the unprocessed raw images. RFP and moxVenus/GFP were pseudo-colored magenta and green respectively.

Protein structure prediction

The structures of Pc12 and Rab13-2 were expected using AlphaFold2 in the Google Colab (https://colab.research.google.com/github/sokrypton/ColabFold/blob/main/AlphaFold2.ipynb#scrollTo=svaADwocVdwl). The predicted proteins were visualized using ChimeraX (Pettersen et al. 2021).

Statistical analysis

Statistical analyses were performed as described in the figure legends. P values were calculated by Student's t-test using GraphPad Prism software.

Data availability

Sequence information of protein-coding genes used in this study was obtained from the FungiDB (https://fungidb.org/), NCBI (https://www.ncbi.nlm.nih.gov/), and Sol Genomics Network (https://solgenomics.net/). The accession numbers for the sequences are as follows: Niben101Scf09596g00001.1 (Rab13-2), Niben101Scf00684g00002.1 (Rab13-3),

Niben101Scf03277g02014.1 (Rab13-4), Niben101Scf05709g00001.1 (Rab13-10), Niben101Scf05032g00003.1 (Rab1), Niben101Scf16705g00001.1 (Rab8B), Niben261Chr06g1220001.1 (REP), and Niben261Chr08g0045015.1 (PRA1). All effector sequence information is included in Supplemental Table 1. Rab13-2 (ID:213473) and constitutively active (ID:213474) or inactive mutant (ID:213475) and the apoplastic marker (ID: 213477) constructs are deposited in Addgene.

Funding

This work was supported by grants from National Research Foundation of Korea (NRF) grants funded by the Korean government (MSIT) (NRF-2018R1A5A1023599 [SRC], NRF-2021R1A2B5B03001613, and NRF-2019R1C1C1008698) to D.C. and US National Science Foundation an NSF awards (NSF EPS-1655726 for E.P.'s start-up and NSF IOS-2126256 to E.P. and J.C.).

AUTHOR CONTRIBUTIONS

E.P. and D.C. conceptualized the project. J.Kim and J.Kaleku performed experiments. H.K., M.K., H.-J.K., and C.S. provided initial data and materials. J.Kim and E.P. analyzed the results. J.Kim, E.P., J.W., and D.C. wrote the manuscript. E.P., J.W., and D.C. provided funding to conduct the project.

Acknowledgements

We thank the INBRE program supported by IDeA from NIGMS, NIH, 2P20GM103432 for providing the spinning disc confocal microscope and Dr. Thomas Boothby to share the LSM 980 confocal microscope.

Declaration of interest

The authors declare no competing interests.

Reference

Adams, C.J., Kopp, M.C., Larburu, N., Nowak, P.R., and Ali, M.M.U. (2019). Structure and molecular mechanism of ER stress signaling by the unfolded protein response signal activator IRE1. Frontiers in Molecular Biosciences **6**.

Alvim, J.C., Bolt, R.M., An, J., Kamisugi, Y., Cuming, A., Silva-Alvim, F.A.L., Concha, J.O., daSilva, L.L.P., Hu, M., Hirsz, D., and Denecke, J. (2023). The K/HDEL receptor does not recycle but instead acts as a Golgi-gatekeeper. Nature Communications **14,** 1612.

Angelos, E., Ruberti, C., Kim, S.-J., and Brandizzi, F. (2017). Maintaining the factory: the roles of the unfolded protein response in cellular homeostasis in plants. The Plant Journal **90,** 671-682.

Balleza, E., Kim, J.M., and Cluzel, P. (2018). Systematic characterization of maturation time of fluorescent proteins in living cells. Nature Methods **15,** 47-51.

Berthold, F., Roujol, D., Hemmer, C., Jamet, E., Ritzenthaler, C., Hoffmann, L., and Schmitt-Keichinger, C. (2019). Inside or outside? A new collection of gateway vectors allowing plant protein subcellular localization or over-expression. Plasmid **105,** 102436.

Boevink, P.C., Birch, P.R.J., Turnbull, D., and Whisson, S.C. (2020). Devastating intimacy: the cell biology of plant–Phytophthora interactions. New Phytologist **228,** 445-458.

Botër, M., Amigues, B.a., Peart, J., Breuer, C., Kadota, Y., Casais, C., Moore, G., Kleanthous, C., Ochsenbein, F., Shirasu, K., and Guerois, R.l. (2007). Structural and functional analysis of SGT1 reveals that its interaction with HSP90 is required for the accumulation of Rx, an R protein involved in plant immunity. The Plant Cell **19,** 3791-3804.

Cao, S.S., and Kaufman, R.J. (2012). Unfolded protein response. Current Biology **22,** R622-R626.

Chaparro-Garcia, A., Wilkinson, R.C., Gimenez-Ibanez, S., Findlay, K., Coffey, M.D., Zipfel, C., Rathjen, J.P., Kamoun, S., and Schornack, S. (2011). The receptor-like kinase SERK3/BAK1 is required for basal resistance against the late blight pathogen *Phytophthora infestans* in *Nicotiana benthamiana*. PLOS ONE **6,** e16608.

Cheng, W., Song, X.-S., Li, H.-P., Cao, L.-H., Sun, K., Qiu, X.-L., Xu, Y.-B., Yang, P.,

Huang, T., Zhang, J.-B., Qu, B., and Liao, Y.-C. (2015). Host-induced gene silencing of an essential chitin synthase gene confers durable resistance to *Fusarium* head blight and seedling blight in wheat. Plant Biotechnology Journal **13,** 1335-1345.

Dongus, J.A., and Parker, J.E. (2021). EDS1 signalling: at the nexus of intracellular and surface receptor immunity. Current Opinion in Plant Biology **62,** 102039.

Fan, G., Yang, Y., Li, T., Lu, W., Du, Y., Qiang, X., Wen, Q., and Shan, W. (2018). A *Phytophthora capsici* RXLR effector targets and inhibits a plant PPIase to suppress endoplasmic reticulum-mediated immunity. Molecular Plant **11,** 1067-1083.

Figueroa, C., Taylor, J., and Vojtek, A.B. (2001). Prenylated Rab acceptor protein is a receptor for prenylated small GTPases. Journal of Biological Chemistry **276,** 28219-28225.

Gray, J.L., von Delft, F., and Brennan, P.E. (2020). Targeting the small GTPase superfamily through their regulatory proteins. Angewandte Chemie International Edition **59,** 6342-6366.

Gu, Y., Zavaliev, R., and Dong, X. (2017). Membrane trafficking in plant immunity. Molecular Plant **10,** 1026-1034.

Guo, Z., Wu, Y.-W., Das, D., Delon, C., Cramer, J., Yu, S., Thuns, S., Lupilova, N., Waldmann, H., Brunsveld, L., Goody, R.S., Alexandrov, K., and Blankenfeldt, W. (2008). Structures of RabGGTase–substrate/product complexes provide insights into the evolution of protein prenylation. The EMBO Journal **27,** 2444-2456.

Hyodo, K., Kaido, M., and Okuno, T. (2014). Traffic jam on the cellular secretory pathway generated by a replication protein from a plant RNA virus. Plant Signaling & Behavior **9,** e28644.

Hyodo, K., Mine, A., Taniguchi, T., Kaido, M., Mise, K., Taniguchi, H., and Okuno, T. (2013). ADP ribosylation factor 1 plays an essential role in the replication of a plant RNA Virus. Journal of Virology **87,** 163-176.

Jumper, J., Evans, R., Pritzel, A., Green, T., Figurnov, M., Ronneberger, O., Tunyasuvunakool, K., Bates, R., Žídek, A., Potapenko, A., Bridgland, A., Meyer, C., Kohl, S.A.A., Ballard, A.J., Cowie, A., Romera-Paredes, B., Nikolov, S., Jain, R., Adler, J., Back, T., Petersen, S., Reiman, D., Clancy, E., Zielinski, M., Steinegger, M.,

Pacholska, M., Berghammer, T., Bodenstein, S., Silver, D., Vinyals, O., Senior, A.W., Kavukcuoglu, K., Kohli, P., and Hassabis, D. (2021). Highly accurate protein structure prediction with AlphaFold. Nature **596,** 583-589.

Kamoun, S., Furzer, O., Jones, J.D.G., Judelson, H.S., Ali, G.S., Dalio, R.J.D., Roy, S.G., Schena, L., Zambounis, A., Panabières, F., Cahill, D., Ruocco, M., Figueiredo, A., Chen, X.-R., Hulvey, J., Stam, R., Lamour, K., Gijzen, M., Tyler, B.M., Grünwald, N.J., Mukhtar, M.S., Tomé, D.F.A., Tör, M., Van Den Ackerveken, G., McDowell, J., Daayf, F., Fry, W.E., Lindqvist-Kreuze, H., Meijer, H.J.G., Petre, B., Ristaino, J., Yoshida, K., Birch, P.R.J., and Govers, F. (2015). The top 10 oomycete pathogens in molecular plant pathology. Molecular Plant Pathology **16,** 413-434.

Kim, J., Park, M., Jeong, E.S., Lee, J.M., and Choi, D. (2017). Harnessing anthocyanin-rich fruit: a visible reporter for tracing virus-induced gene silencing in pepper fruit. Plant Methods **13,** 3.

Ko, D.K., Kim, J.Y., Thibault, E.A., and Brandizzi, F. (2023). An IRE1-proteasome system signalling cohort controls cell fate determination in unresolved proteotoxic stress of the plant endoplasmic reticulum. Nature Plants **9,** 1333-1346.

Lamour, K.H., Stam, R., Jupe, J., and Huitema, E. (2012). The oomycete broad-host-range pathogen *Phytophthora capsici*. Molecular Plant Pathology **13,** 329-337.

Lee, S., Kim, J., Kim, M.-S., Min, C.W., Kim, S.T., Choi, S.-B., Lee, J.H., and Choi, D. (2023). The *Phytophthora* nucleolar effector Pi23226 targets host ribosome biogenesis to induce necrotrophic cell death. Plant Communications **4,** 100606.

Lee, S., Lee, Y.J., Choi, S., Park, S.-B., Tran, Q.-G., Heo, J., and Kim, H.-S. (2018). Development of an alcohol-inducible gene expression system for recombinant protein expression in *Chlamydomonas reinhardtii*. Journal of Applied Phycology **30,** 2297-2304.

Li, Q., Ai, G., Shen, D., Zou, F., Wang, J., Bai, T., Chen, Y., Li, S., Zhang, M., Jing, M., and Dou, D. (2019). A *Phytophthora capsici* effector targets ACD11 binding partners that regulate ROS-mediated defense response in *Arabidopsis*. Molecular Plant **12,** 565-581.

Li, T., Ai, G., Fu, X., Liu, J., Zhu, H., Zhai, Y., Pan, W., Shen, D., Jing, M., Xia, A., and

Dou, D. (2022). A *Phytophthora capsici* RXLR effector manipulates plant immunity by targeting RAB proteins and disturbing the protein trafficking pathway. Molecular Plant Pathology **23,** 1721-1736.

Liu, J.-X., and Howell, S.H. (2016). Managing the protein folding demands in the endoplasmic reticulum of plants. New Phytologist **211,** 418-428.

McLellan, H., Harvey, S.E., Steinbrenner, J., Armstrong, M.R., He, Q., Clewes, R., Pritchard, L., Wang, W., Wang, S., Nussbaumer, T., Dohai, B., Luo, Q., Kumari, P., Duan, H., Roberts, A., Boevink, P.C., Neumann, C., Champouret, N., Hein, I., Falter-Braun, P., Beynon, J., Denby, K., and Birch, P.R.J. (2022). Exploiting breakdown in nonhost effector–target interactions to boost host disease resistance. Proceedings of the National Academy of Sciences **119,** e2114064119.

Nelson, B.K., Cai, X., and Nebenführ, A. (2007). A multicolored set of in vivo organelle markers for co-localization studies in *Arabidopsis* and other plants. The Plant journal **51,** 1126-1136.

Nielsen, E. (2020). The small GTPase superfamily in plants: A conserved regulatory module with novel functions. Annual Review of Plant Biology **71,** 247-272.

Nielsen, E., Cheung, A.Y., and Ueda, T. (2008). The regulatory RAB and ARF GTPases for vesicular trafficking. Plant Physiology **147,** 1516-1526.

Niu, T.-K., Pfeifer, A.C., Lippincott-Schwartz, J., and Jackson, C.L. (2005). Dynamics of GBF1, a brefeldin A-sensitive Arf1 exchange factor at the Golgi. Molecular Biology of the Cell **16,** 1213-1222.

Oakes, S.A., and Papa, F.R. (2015). The role of endoplasmic reticulum stress in human pathology. Annual Review of Pathology: Mechanisms of Disease **10,** 173-194.

Pandey, P., Leary, A.Y., Tumtas, Y., Savage, Z., Dagvadorj, B., Duggan, C., Yuen, E.L.H., Sanguankiattichai, N., Tan, E., Khandare, V., Connerton, A.J., Yunusov, T., Madalinski, M., Mirkin, F.G., Schornack, S., Dagdas, Y., Kamoun, S., and Bozkurt, T.O. (2021). An oomycete effector subverts host vesicle trafficking to channel starvation-induced autophagy to the pathogen interface. eLife **10,** e65285.

Parada-Rojas, C.H., Granke, L.L., Naegele, R.P., Hansen, Z., Hausbeck, M.K., Kousik, C.S., McGrath, M.T., D. Smart, C., and Quesada-Ocampo, L.M. (2021). A diagnostic guide for *Phytophthora capsici* infecting vegetable crops. Plant Health Progress **22,** 404-414.

Park, E., Lee, H.-Y., Woo, J., Choi, D., and Dinesh-Kumar, S.P. (2017). Spatiotemporal monitoring of *Pseudomonas syringae* effectors via type III secretion using split fluorescent protein fragments. The Plant Cell **29,** 1571-1584.

Petre, B., Contreras, M.P., Bozkurt, T.O., Schattat, M.H., Sklenar, J., Schornack, S., Abd-El-Haliem, A., Castells-Graells, R., Lozano-Durán, R., Dagdas, Y.F., Menke, F.L.H., Jones, A.M.E., Vossen, J.H., Robatzek, S., Kamoun, S., and Win, J. (2021). Host-interactor screens of *Phytophthora infestans* RXLR proteins reveal vesicle trafficking as a major effector-targeted process. The Plant Cell **33,** 1447-1471.

Pylypenko, O., Hammich, H., Yu, I.M., and Houdusse, A. (2018). Rab GTPases and their interacting protein partners: structural insights into Rab functional diversity. Small GTPases **9,** 22-48.

Qiang, X., Zechmann, B., Reitz, M.U., Kogel, K.-H., and Schäfer, P. (2012). The mutualistic fungus *Piriformospora indica* colonizes *Arabidopsis* roots by inducing an endoplasmic reticulum stress–triggered caspase-dependent cell death The Plant Cell **24,** 794-809.

Quesada-Ocampo, L.M., Parada-Rojas, C.H., Hansen, Z., Vogel, G., Smart, C., Hausbeck, M.K., Carmo, R.M., Huitema, E., Naegele, R.P., Kousik, C.S., Tandy, P., and Lamour, K. (2023). *Phytophthora capsici*: recent progress on fundamental biology and disease management 100 years after its description. Annual Review of Phytopathology **61,** 185-208.

Reyes-Tena, A., Huguet-Tapia, J.C., Lamour, K.H., Goss, E.M., Rodríguez-Alvarado, G., Vázquez-Marrufo, G., Santillán-Mendoza, R., and Fernández-Pavía, S.P. (2019). Genome sequence data of six isolates of *Phytophthora capsici* from Mexico. Molecular Plant-Microbe Interactions **32,** 1267-1269.

Schultink, A., Qi, T., Lee, A., Steinbrenner, A.D., and Staskawicz, B. (2017). Roq1 mediates recognition of the *Xanthomonas* and *Pseudomonas* effector proteins XopQ and

HopQ1. The Plant Journal **92,** 787-795.

Seo, Y.-E., Lee, H.-Y., Kim, H., Yan, X., Park, S.A., Kim, M.-S., Segonzac, C., Choi, D., and Mang, H. (2022). The *Phytophthora capsici* RxLR effector CRISIS2 triggers cell death via suppressing plasma membrane H^+-ATPase in the host plant. Journal of Experimental Botany **74,** 1675-1689.

Simoni, E.B., Oliveira, C.C., Fraga, O.T., Reis, P.A.B., and Fontes, E.P.B. (2022). Cell death signaling from endoplasmic reticulum stress: plant-specific and conserved features. Frontiers in Plant Science **13**.

Stenmark, H. (2009). Rab GTPases as coordinators of vesicle traffic. Nature Reviews Molecular Cell Biology **10,** 513-525.

Tomczynska, I., Stumpe, M., and Mauch, F. (2018). A conserved RxLR effector interacts with host RABA-type GTPases to inhibit vesicle-mediated secretion of antimicrobial proteins. The Plant Journal **95,** 187-203.

Wawra, S., Trusch, F., Matena, A., Apostolakis, K., Linne, U., Zhukov, I., Stanek, J., Koźmiński, W., Davidson, I., Secombes, C.J., Bayer, P., and van West, P. (2017). The RxLR motif of the host targeting effector AVR3a of *Phytophthora infestans* is cleaved before secretion. The Plant Cell **29,** 1184-1195.

Whisson, S.C., Boevink, P.C., Moleleki, L., Avrova, A.O., Morales, J.G., Gilroy, E.M., Armstrong, M.R., Grouffaud, S., van West, P., Chapman, S., Hein, I., Toth, I.K., Pritchard, L., and Birch, P.R.J. (2007). A translocation signal for delivery of oomycete effector proteins into host plant cells. Nature **450,** 115-118.

Wu, C.-H., Abd-El-Haliem, A., Bozkurt, T.O., Belhaj, K., Terauchi, R., Vossen, J.H., and Kamoun, S. (2017). NLR network mediates immunity to diverse plant pathogens. Proceedings of the National Academy of Sciences **114,** 8113-8118.

Yang, Y., Liu, X., Zhang, W., Qian, Q., Zhou, L., Liu, S., Li, Y., and Hou, X. (2021). Stress response proteins NRP1 and NRP2 are pro-survival factors that inhibit cell death during ER stress. Plant Physiology **187,** 1414-1427.

Yang, Z.-T., Wang, M.-J., Sun, L., Lu, S.-J., Bi, D.-L., Sun, L., Song, Z.-T., Zhang, S.-S.,

766 **Zhou, S.-F., and Liu, J.-X.** (2014). The membrane-associated transcription factor NAC089
767 controls ER-stress-induced programmed cell death in plants. PLOS Genetics **10,** e1004243.

768 **Yuen, E.L.H., Shepherd, S., and Bozkurt, T.O.** (2023). Traffic control: subversion of plant
769 membrane trafficking by pathogens. Annual Review of Phytopathology **61,** null.

Figure and table legends

Figure 1. Pc12 causes cell death independent of defense response in *Solanaceae*.

(A) Pc12-triggered cell death in *Nicotiana benthamiana, Nicotiana tobacum, Capsicum annuum*, and *Solanaceae lycopersicum*. Bax and EGFP were used as a positive control and a negative control, respectively. The leaves of 4-week-old of plants were agroinfiltrated. The images were photographed under white and UV light at 2 days after agroinfiltration.

(B) Cell death induced by Pc12 in *N. benthamiana* with silenced NLR-downstream signaling genes *EDS1*, *ADR1/NRG1*, *NRC2/3/4*, and *SGT.* Positive controls consisted of the combinations Rpiblb2+Avrblb2, R3a+Avr3a, R8+Avr8, and N+p50, while GFP served as the negative control. Agrobacterium carrying each construct was infiltrated into the leaves of 5-week-old plants with the respective gene components silenced, and images were taken at 2 dpi.

(C) Cell death observed in images (B) was quantified using the quantum yield (*Fv/Fm*) using a closed FluorCam system. The data represents the mean ± standard deviation (SD, n = 7-10). a indicates statistically significant differences by Student t-test (****, $P < 0.0001$).

(D) qRT-PCR analysis of the transcripts level in *N. benthamiana*-silencing *SGT1, EDS1, ADR1/NRG1,* and *NRC2/3/4.* Leaf disks were sampled at 5-week-old in each components-silenced *N. benthamiana.* Asterisks denote statistically significant differences by Student t-test (****, $P < 0.0001$). Data are mean ± SD.

(E) Expression patterns of *PR1, RbohB*, and *WKRY8* in *N. benthamiana* expressing Pc12, XopQ, and empty vector (EV). Total RNA was extracted in 30 hour-post-infiltration. Asterisks denote statistically significant differences by Student t-test (*, $P < 0.1$; **, $P < 0.01$; ***, $P < 0.001$; ****, $P < 0.0001$). Data are mean ± SD. (3 experimental repeats).

Figure 2. Pc12 enhances the growth of *P. capsici*, triggering necrotic cell death through its C-terminus.

(A) Increased growth of *P. capsici* under Pc12 expression compared to a control. RFP and RFP-Pc12 were expressed by ethanol-inducible promoter in *N. benthamiana*. *P. capsici* was inoculated on the leaves at 1 day-post-agroinfiltration without ethanol treatment. Images were taken under UV light at 2 day post-inoculation. The lesion sizes were measured using ImageJ. Asterisks denote statistically significant differences using a Student t-test (****, $P < 0.0001$).

Data are mean ± SD.

(B) Relative biomass of *P. capsici* in the leaves shown in Figure 2A. Leaf disks from around the inoculated area were sampled at 2 dpi. Total genomic DNA was extracted and subjected to qPCR analysis. The *P. capsici* biomass was quantified by the *PcActin* normalized to the *NbEF1α*. Asterisks denote statistically significant differences by Student t-test (****, $P < 0.0001$). Data are mean ± SD.

(C) Suppression of *P. capsici* symptoms through Pc12 silencing via HIGS. Plants were agroinfiltrated with TRV carrying GFP and Pc12. At 14 dpi, *P. capsici* was inoculated on the upper leaves. Images were taken at 2 dpi, and the lesion size was measured by ImageJ.

(D) Relative expression of Pc12 in Pc12-silenced and GFP leaves. The inoculated leaves were sampled at 6 hpi and utilized in qRT-PCR analysis. The transcripts level of Pc12 was normalized to the *PcTubulin*. Asterisks denote statistically significant differences by Student t-test (**, $P < 0.01$; ****, $P < 0.0001$). Data are mean ± SD.

(E) Pairwise sequence alignment comparisons of Pc12 homologs of *P. capsici* genome (LT1534). Alignments were obtained using the MUSCLE algorithm and were visualized via ESPript 3.0 (Robert and Gouet 2014). Strictly or highly conserved residues are highlighted in red boxes or blue empty boxes, respectively.

(F) Schematic representation of C-terminal chimeras between Pc12 and Pc22034.

(G) Cell death induced by the Pc12, Pc22034, Pc22034 mutants, and Pc12ΔC5 described in (F)

Figure 3. The Pc12 family interacts with the small GTPase Rab13-2 homologs, directly binding to its active form.

(A) Rab13-2 interacts with Pc12 homologs, inducing cell death. Rab13-2, with a N-terminal GFP, and 3xHA-Pc12 were transiently expressed in plants. Leaf samples were sampled at 30 hpi. Total protein extracts were subjected to co-IP using anti GFP agarose beads. (3 experimental repeats)

(B) Pc12 interacts with the subclade including Rab13-2, -3, and -4. The plants were transiently expressing 3xHA-Pc12 and GFP-Rab13 homologs and sampled at 30 hpi. (3 experimental repeats)

(C) Interaction of Pc12 with Rab13-2 and Rab13-2^{Q74L}, not Rab13-2^{S29N} *in planta*. Pc12 and Pc12ΔC5 were transiently co-expressed with Rab13-2, Rab13-2^{Q74L}, and Rab13-2^{S29N} in *N.*

benthamiana.

(D) Physical interaction of Pc12 with Rab13-2 and Rab13-2^{Q74L}, not Rab13-2^{S29N} *in vivo*. Yeast cells transformed with GAL4BD-Pc12 or Pc12ΔC5 and GAL4AD-Rab13-2 or mutants were grown on synthetic media lacking LTH or LT for 7 days. The combination of GAL4BD-p53 and GAL4AD-T was used as a positive control.

Figure 4. Pc12 relocates Rab13-2 and enhances the interaction between Rab13-2 and REP by mimicking the inactive state of Rab13-2.

(A) Pc12 and Pc12ΔC5 are localized in the cytoplasm. GFP-Pc12 as well as GFP- Pc12ΔC5, a control GFP were infiltrated in the leaves of a transgenic *N. benthamiana* expressing RFP-HDEL as an ER marker (Magenta). Transient expressions of those proteins were imaged by a spinning disc confocal microscope. More than 60 z-images in 0.3 μm step size were superimposed by a maximum z-projection function in ImageJ. The brightness of the original micrograms was enhanced to improve the visibility of subcellular compartments. This processing does not change the conclusion drawn from the images. GFP was pseudo-colored to green, while RFP displayed in magenta. More than 12 images were acquired from 3 independent experiments. Scale bars, 20 μm.

(B) Localization of Rab13-2 mutants in ER-marker transgenic *N. benthamiana. Agrobacteria* containing GFP-Rab13-2, GFP- Rab13-2^{Q74L}, or GFP-Rab13-2^{S29N} expression cassettes were infiltrated in the leaves of the ER-marker transgenic *N. benthamiana*. Transient expressions of those proteins in the leaf epidermal cells were imaged by a spinning disc confocal microscope. More than 60 z-images in 0.3 μm step size were superimposed by a maximum z-projection function in ImageJ. The brightness of the original micrograms was enhanced to improve the visibility of subcellular compartments. This processing does not change the conclusion drawn from the images. GFP was pseudo-colored to green, while RFP displayed in magenta. More than 12 images were acquired from 3 independent experiments. Scale bars, 20 μm.

(C) Co-IP assays showing that Pc12 increased binding affinity between Rab13-2 and REP. The plants transiently expressing GFP-Rab13-2, REP- or PRA1-3xFLAG, and RFP or RFP-Pc12 were sampled at 1 day after a 10% ethanol treatment at 1 day-post-agroinfiltration. Total protein extracts were subjected to co-IP using anti GFP agarose beads. The precipitated proteins were immunoblotted. The level of binding was calculated as the ratio between anti-FLAG and anti-

FLAG of IP by imageJ. Red asterisks indicate expected band sizes.

(D) Pc12 strengthen the weak interaction between REP and Rab13-2^{Q74L}. The plants were infiltrated with an agrobacterium carrying REP-3xFLAG and an agrobacterium containing two plasmids, one plasmid with RFP or RFP-Pc12 and the other with GFP-Rab13-2^{Q74L} or Rab13-2^{S29N}, in a 1:1 ratio in *N. benthamiana*. Samples treated with 10% ethanol at 1 dpi were collected at 12 hours post treatment. The level of binding was calculated as the ratio between anti-FLAG and anti-FLAG of IP by imageJ. Red asterisks indicate expected RFP and RFP-Pc12 band sizes.

(E) Altered localization of Rab13-2 mutants by the co-expression of RFP-Pc12. Cytosolic diffusion of GFP-Rab13-2^{Q74L} was altered to show punctate localization frequently (yellow arrows), while Golgi localization of GFP-Rab13-2^{S29N} were inhibited by the co-expression of Pc12 (white arrowheads). The brightness of the original micrograms was enhanced to improve the visibility of subcellular compartments. More than 60 z-images in 0.3 μm step size were superimposed by a maximum z-projection function in ImageJ. This processing does not change the conclusion drawn from the images. GFP was pseudo-colored to green, while RFP displayed in magenta. More than 12 images were acquired from 3 independent experiments. Scale bars, 20 μm.

Figure 5. Pc12 inhibits the location of ER-resident RFP and the secretion of apoplastic membrane-anchored moxVenus, triggering ER stress separate from the effects of tunicamycin.

(A) Discontinuity and puncta localization of RFP-HDEL under the expression of Pc12. GFP, GFP-Pc12 and GFP-Pc12ΔC5 were transiently expressed in transgenic *N. benthamiana* expressing RFP-HDEL. More than 60 z-images in 0.3 μm step size were acquired by a spinning disc confocal microscope. Images were superimposed by a maximum z-projection function in ImageJ. The brightness of the original micrograms was enhanced to improve the visibility of subcellular compartments. This processing does not change the conclusion drawn from the images. RFP displayed in magenta. More than 12 images were acquired from 3 independent experiments. Scale bars, 20 μm.

(B) Apoplastic membrane targeted moxVenus (apoSP-moxVenus-TM) remained in ER in the existence of Pc12. RFP-Pc12, RFP- Pc12ΔC5, and RFP driven by the ethanol promoter were

induced by 10% ethanol treatment. Pc12 expression inhibited the secretion of the marker proteins resulted in their accumulation in the ER. Z-images for thicker than 3 μm sections in 0.75 μm step size were acquired by a laser scanning confocal microscope. Images of the corresponding sections were processed to improve the brightness for the clarity. This processing does not change the conclusion drawn from the images. moxVenus was pseudo-colored to green. More than 12 images were acquired from 3 independent experiments. Scale bars, 20 μm.

(C) Accumulation of the ER stress marker protein (Bip) in response to Pc12 expression. Plants were treated with mock and Tm (10 ug/ml) and sampled over time. Plants expressing RFP and RFP-Pc12 after 5% ethanol treatment were sampled over time.

(D) Transcripts level of UPR-related transcription factor and ER chaperon genes upon expression of Pc12. In (C), total RNA was extracted at 0 and 12 hours after tunicamycin or ethanol treatment. UPR-related genes, ER chaperon genes (*BLP4* and *CRT1*) and transcription factor genes (*bZIP28* and *bZIP60*), were normalized with *NbEF1a* in qRT-PCR.

Figure 6. A mutation in a key Rab13-2 residue weakens Pc12 binding without affecting REP and PRA1 binding, compromising *P. capsici* virulence.

(A-B) The predicted structures of Pc12 and Rab13-2 interaction by AlphaFold2. (B) zooms in on the black box in (A). The green lines depict the intracellular bonds between Pc12 and Rab13-2.

(C - E) *In planta*, a co-immunoprecipitation assay with Rab13-2, Rab13-2^{T47A}, and Pc12 (REP or PRA1). Total protein extracts were precipitated with anti HA magnetic beads or anti FLAG agarose. The precipitated protein and total protein were detected by western blotting.

(F) *P. capsici* inoculation on the leaves expressing GFP-Rab13-2 and GFP-Rab13-2^{T47A}. Agrobacterium carrying GFP-Rab13-2 and GFP-Rab13-2^{T47A} was infiltrated in *N. benthamiana,* followed by *P. capsici* inoculation at 1 dpi. Images were taken at 72 hpi, and the lesion size was measured by ImageJ (N = 31 - 32, 3 repeats).

Figure 7. Summary model of the inhibition of Pc12 in Rab13-2-mediated vesicle trafficking.

Prenylated Rab13-2 in its GDP-bound state is inserted to a membrane by Rab escort protein

(REP). The guanine nucleotide exchange factor (GEF) exchanges GDP for GTP on Rab13-2 to initiate vesicle formation for vesicle trafficking. Pc12, secreted from *P. capsici*, binds to GTP-bound Rab13-2, subsequently recruiting REP to facilitate the extraction of the complex from the membrane or its retention on the membrane, consequently impeding vesicle formation mediated by Rab13-2. Figure was created using BioRender.com.

Supplemental data

Supplemental Table S1.

Pc12 family in *P. capsici* isolates genome

Supplemental Table S2.

Candidates targeted by Pc12 in Mass spectrometry analysis

Supplemental Table S3.

Rab13-2 interactors from STRING

Supplemental Table S4.

Primer sequences used in this study

Supplemental Figure S1. The expression pattern of Pc12 during the infection phases of *P. capsici.* *PcHmp1* and *PcNpp1* are utilized as markers for the biotrophic and necrotrophic phases, respectively. Leaf disks were sampled at regular time intervals. Each gene is normalized to *PcTubulin*.

Supplemental Figure S2. Pc12 homologs from *P. capsici* induce cell death, except for PHYCA22034.

(A) Cell death analysis of Pc12 homologs from *P. capsici, P. ramorum, P. cinnamoni,* and *P. sojae.* Pc12 homologs were expressed in 4-week-old *N. benthamiana* and images were photographed at 2 day after agroinfiltration.

(B) The cell death in images (A) was quantified by quantum yield (*Fv/Fm*) using a closed FluorCam system. Data are mean ± SD (n = 9-12). a indicates statistically significant differences by Student t-test (a, $P < 0.0001$).

Supplemental Figure S3. Phylogeny tree of Rab family in *N. benthamiana.*

The red triangle represents the Pc12 target detected in MS, while black triangles represent Rab proteins used in the Co-IP shown in Figure 3B.

Supplemental Figure S4.

Localization of Rab13-2 at Golgi apparatus. GFP-Rab13-2 were co-expressing with a Golgi marker in plants, which were observed at 2 dpi.

Supplemental Figure S5. REP and PRA1 prefer to interact the inactive form of Rab13-2 (Rab13-2^{S29N}).

Leaves expressing REP or PRA1 with Rab13-2 mutants were sampled at 2 dpi, and total protein extracts were subjected to co-IP using anti-FLAG agarose beads. (3 experimental repeats)

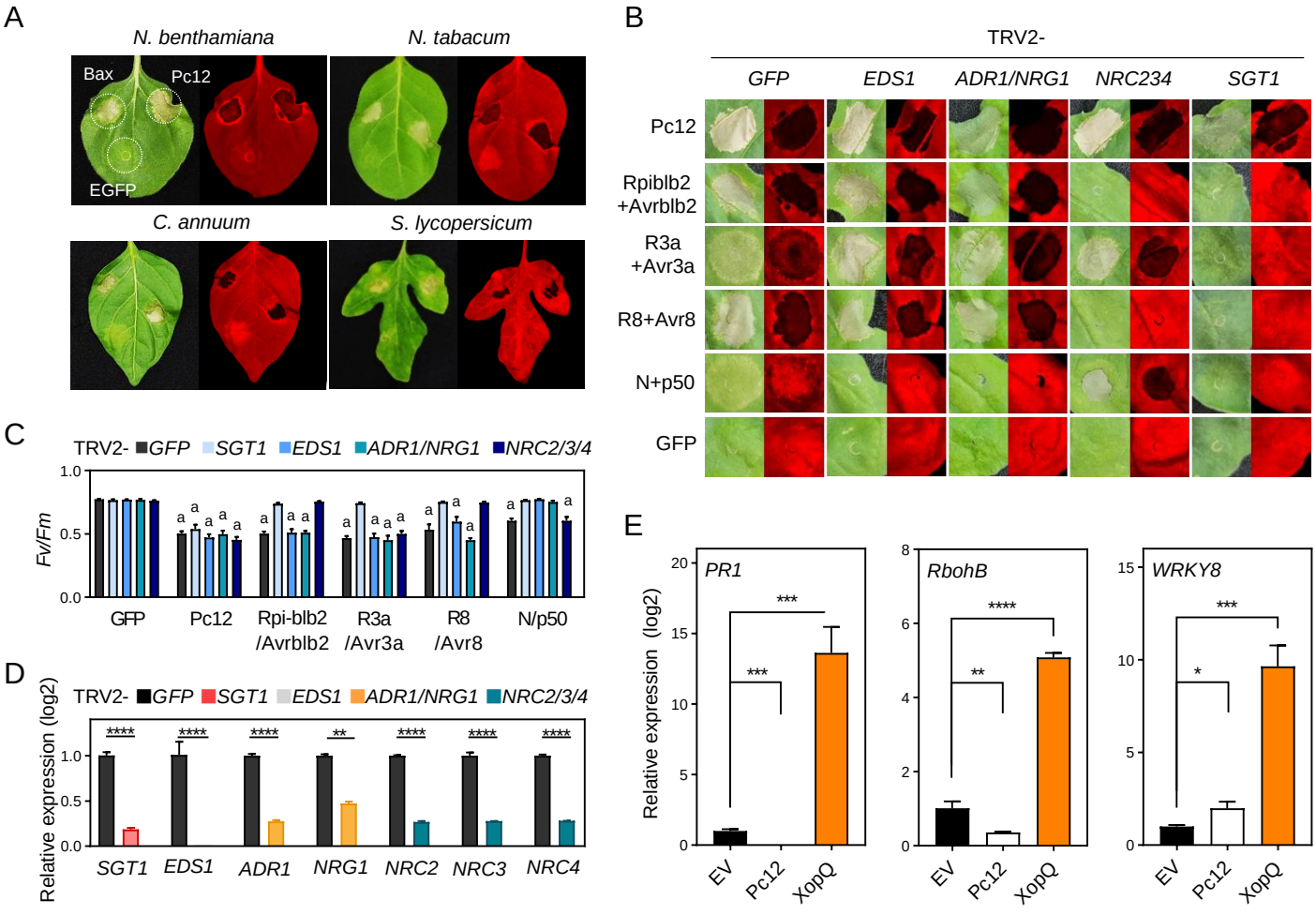

Figure 1. Pc12 causes cell death independent of defense response in *Solanaceae*.

(A) Pc12-triggered cell death in *Nicotiana benthamiana, Nicotiana tobacum, Capsicum annuum*, and *Solanaceae lycopersicum*. Bax and EGFP were used as a positive control and a negative control, respectively. The leaves of 4-week-old of plants were agroinfiltrated. The images were photographed under white and UV light at 2 days after agroinfiltration.

(B) Cell death induced by Pc12 in *N. benthamiana* with silenced NLR-downstream signaling genes *EDS1*, *ADR1/NRG1*, *NRC2/3/4*, and *SGT.* Positive controls consisted of the combinations Rpiblb2+Avrblb2, R3a+Avr3a, R8+Avr8, and N+p50, while GFP served as the negative control. Agrobacterium carrying each construct was infiltrated into the leaves of 5-week-old plants with the respective gene components silenced, and images were taken at 2 dpi.

(C) Cell death observed in images (B) was quantified using the quantum yield (*Fv/Fm*) using a closed FluorCam system. The data represents the mean ± standard deviation (SD, n = 7-10). a indicates statistically significant differences by Student t-test (****, P < 0.0001).

(D) qRT-PCR analysis of the transcripts level in *N. benthamiana*-silencing *SGT1, EDS1, ADR1/NRG1,* and *NRC2/3/4.* Leaf disks were sampled at 5-week-old in each components-silenced *N. benthamiana.* Asterisks denote statistically significant differences by Student t-test (****, P < 0.0001). Data are mean ± SD.

(E) Expression patterns of *PR1, RbohB*, and *WKRY8* in *N. benthamiana* expressing Pc12, XopQ, and empty vector (EV). Total RNA was extracted in 30 hour-post-infiltration. Asterisks denote statistically significant differences by Student t-test (*, P < 0.1; **, P < 0.01; ***, P < 0.001; ****, P < 0.0001). Data are mean ± SD. (3 experimental repeats).

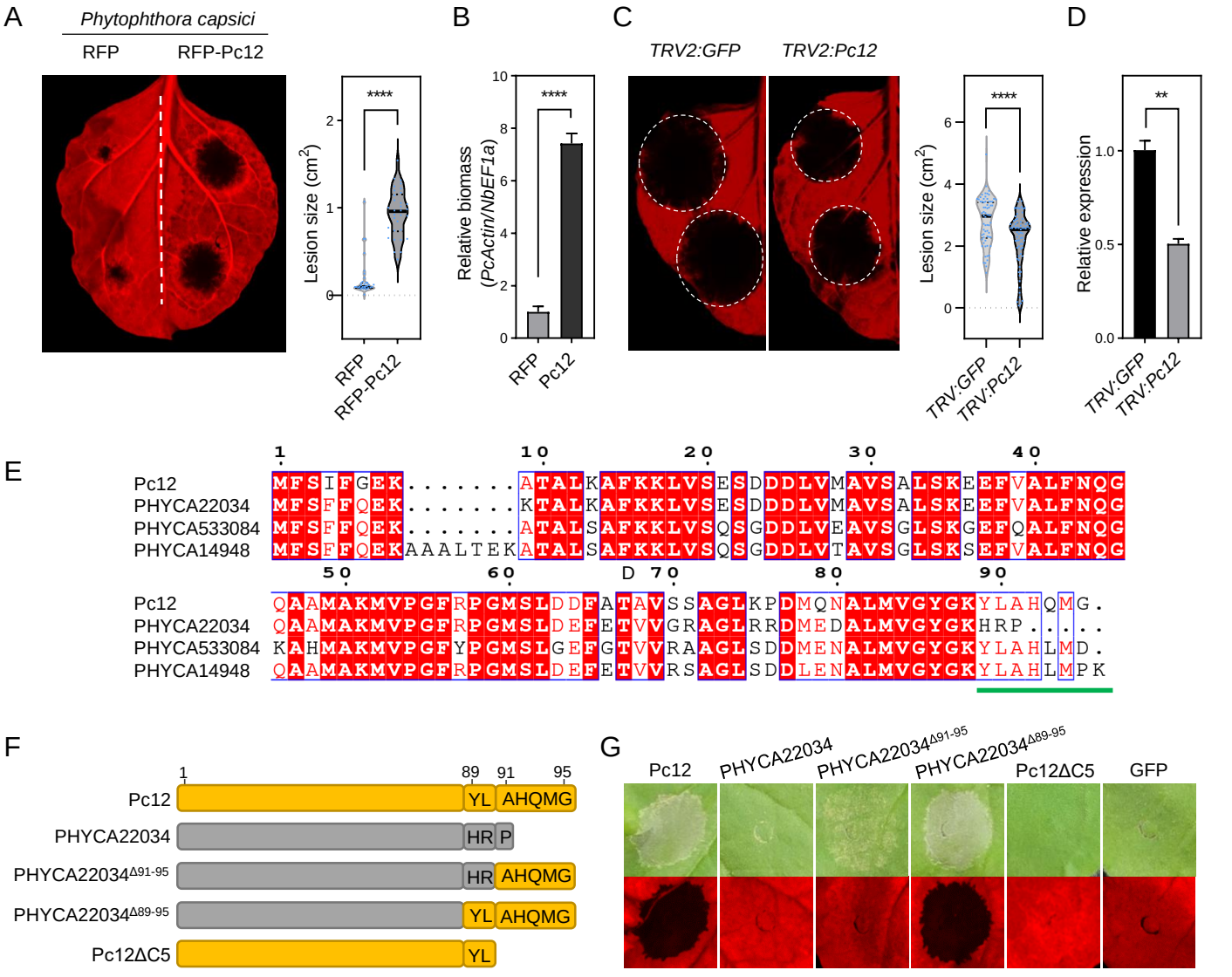

Figure 2. Pc12 enhances the growth of *P. capsici*, triggering necrotic cell death through its C-terminus.
(A) Increased growth of *P. capsici* under Pc12 expression compared to a control. RFP and RFP-Pc12 were expressed by ethanol-inducible promoter in *N. benthamiana*. *P. capsici* was inoculated on the leaves at 1 day-post-agroinfiltration without ethanol treatment. Images were taken under UV light at 2 day post-inoculation. The lesion sizes were measured using ImageJ. Asterisks denote statistically significant differences using a Student t-test (****, P < 0.0001). Data are mean ± SD.
(B) Relative biomass of *P. capsici* in the leaves shown in Figure 2A. Leaf disks from around the inoculated area were sampled at 2 dpi. Total genomic DNA was extracted and subjected to qPCR analysis. The *P. capsici* biomass was quantified by the *PcActin* normalized to the *NbEF1α*. Asterisks denote statistically significant differences by Student t-test (****, P < 0.0001). Data are mean ± SD.
(C) Suppression of *P. capsici* symptoms through Pc12 silencing via HIGS. Plants were agroinfiltrated with TRV carrying GFP and Pc12. At 14 dpi, *P. capsici* was inoculated on the upper leaves. Images were taken at 2 dpi, and the lesion size was measured by ImageJ.
(D) Relative expression of Pc12 in Pc12-silenced and GFP leaves. The inoculated leaves were sampled at 6 hpi and utilized in qRT-PCR analysis. The transcripts level of Pc12 was normalized to the *PcTubulin*. Asterisks denote statistically significant differences by Student t-test (**, P < 0.01; ****, P < 0.0001). Data are mean ± SD.
(E) Pairwise sequence alignment comparisons of Pc12 homologs of *P. capsici* genome (LT1534). Alignments were obtained using the MUSCLE algorithm and were visualized via ESPript 3.0 (Robert and Gouet 2014). Strictly or highly conserved residues are highlighted in red boxes or blue empty boxes, respectively.
(F) Schematic representation of C-terminal chimeras between Pc12 and Pc22034.
(G) Cell death induced by the Pc12, Pc22034, Pc22034 mutants, and Pc12ΔC5 described in (F)

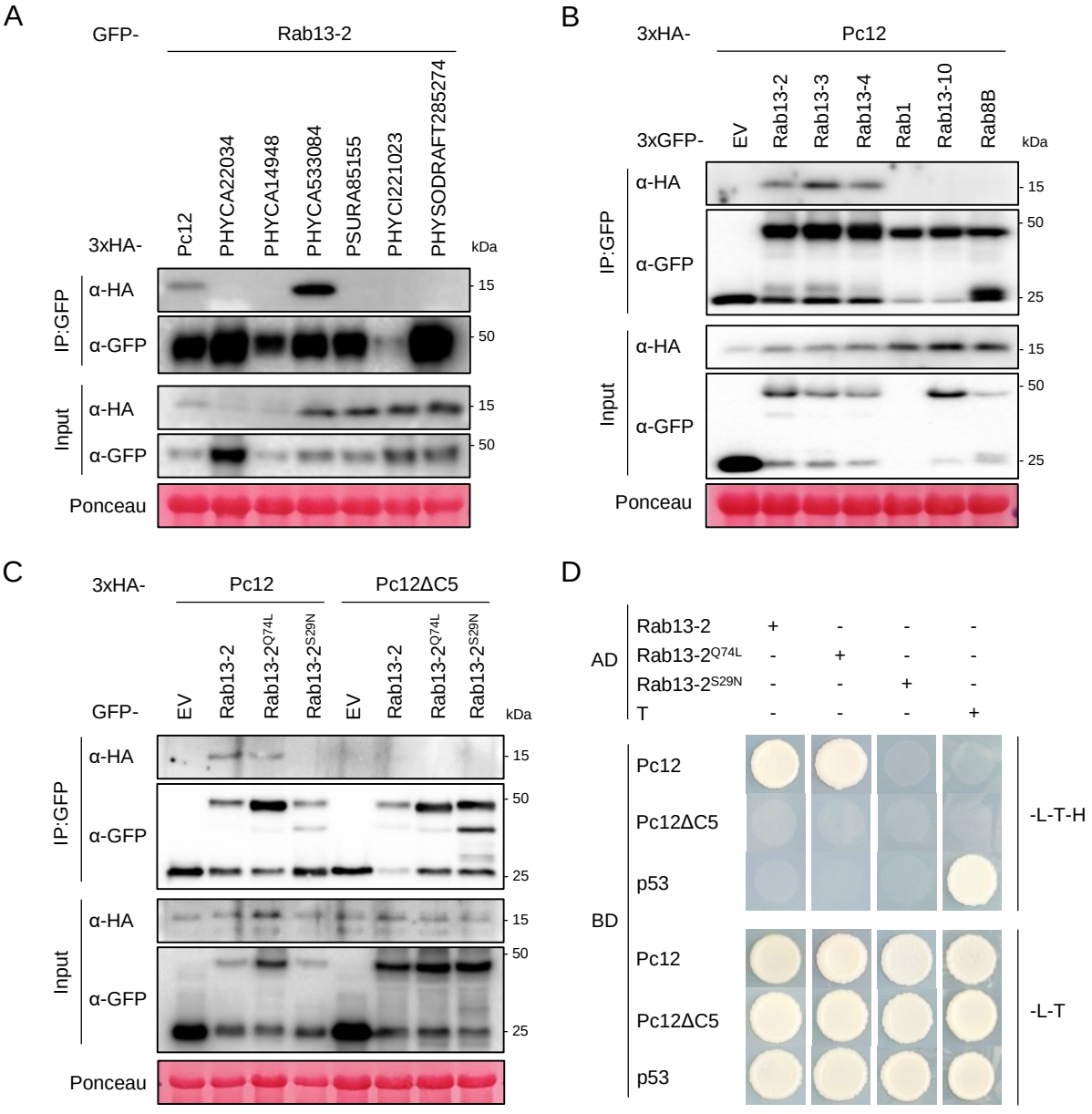

Figure 3 The Pc12 family interacts with the small GTPase Rab13-2 homologs, directly binding to its active form.

(A) Rab13-2 interacts with Pc12 homologs, inducing cell death. Rab13-2, with a N-terminal GFP, and 3xHA-Pc12 were transiently expressed in plants. Leaf samples were sampled at 30 hpi. Total protein extracts were subjected to co-IP using anti GFP agarose beads. (3 experimental repeats)

(B) Pc12 interacts with the subclade including Rab13-2, -3, and -4. The plants were transiently expressing 3xHA-Pc12 and GFP-Rab13 homologs and sampled at 30 hpi. (3 experimental repeats)

(C) Interaction of Pc12 with Rab13-2 and Rab13-2^{Q74L}, not Rab13-2^{S29N} *in planta*. Pc12 and Pc12ΔC5 were transiently co-expressed with Rab13-2, Rab13-2^{Q74L}, and Rab13-2^{S29N} in *N. benthamiana*.

(D) Physical interaction of Pc12 with Rab13-2 and Rab13-2^{Q74L}, not Rab13-2^{S29N} *in vivo*. Yeast cells transformed with GAL4BD-Pc12 or Pc12ΔC5 and GAL4AD-Rab13-2 or mutants were grown on synthetic media lacking LTH or LT for 7 days. The combination of GAL4BD-p53 and GAL4AD-T was used as a positive control.

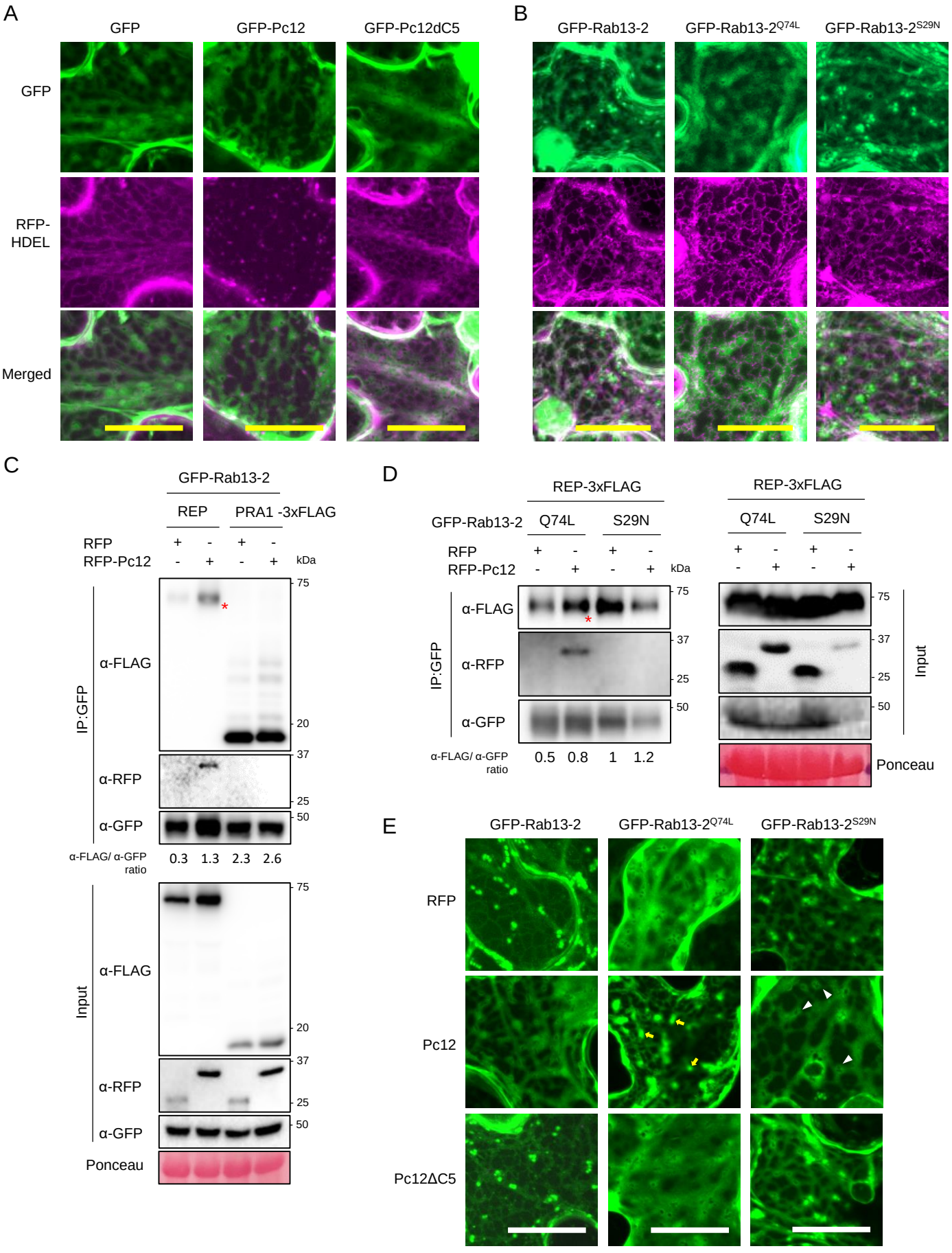
A
GFP
GFP-Pc12
GFP-Pc12dC5
GFP
RFP-HDEL
Merged
B
GFP-Rab13-2
GFP-Rab13-2Q74L
GFP-Rab13-2S29N
C
GFP-Rab13-2
REP
PRA1 -3xFLAG
RFP
RFP-Pc12
kDa
IP:GFP
α-FLAG
α-RFP
α-GFP
α-FLAG/ α-GFP ratio
0.3 1.3 2.3 2.6
Input
Ponceau
D
REP-3xFLAG
GFP-Rab13-2
Q74L
S29N
0.5 0.8 1 1.2
Input
E
GFP-Rab13-2
GFP-Rab13-2Q74L
GFP-Rab13-2S29N
RFP
Pc12
Pc12ΔC5

Figure 4.

Figure 4. Pc12 relocates Rab13-2 and enhances the interaction between Rab13-2 and REP by mimicking the inactive state of Rab13-2.

(A) Pc12 and Pc12ΔC5 are localized in the cytoplasm. GFP-Pc12 as well as GFP- Pc12ΔC5, a control GFP were infiltrated in the leaves of a transgenic *N. benthamiana* expressing RFP-HDEL as an ER marker (Magenta). Transient expressions of those proteins were imaged by a spinning disc confocal microscope. More than 60 z-images in 0.3 μm step size were superimposed by a maximum z-projection function in ImageJ. The brightness of the original micrograms was enhanced to improve the visibility of subcellular compartments. This processing does not change the conclusion drawn from the images. GFP was pseudo-colored to green, while RFP displayed in magenta. More than 12 images were acquired from 3 independent experiments. Scale bars, 20 μm.

(B) Localization of Rab13-2 mutants in ER-marker transgenic *N. benthamiana. Agrobacteria* containing GFP-Rab13-2, GFP- Rab13-2^{Q74L}, or GFP-Rab13-2^{S29N} expression cassettes were infiltrated in the leaves of the ER-marker transgenic *N. benthamiana*. Transient expressions of those proteins in the leaf epidermal cells were imaged by a spinning disc confocal microscope. More than 60 z-images in 0.3 μm step size were superimposed by a maximum z-projection function in ImageJ. The brightness of the original micrograms was enhanced to improve the visibility of subcellular compartments. This processing does not change the conclusion drawn from the images. GFP was pseudo-colored to green, while RFP displayed in magenta. More than 12 images were acquired from 3 independent experiments. Scale bars, 20 μm.

(C) Co-IP assays showing that Pc12 increased binding affinity between Rab13-2 and REP. The plants transiently expressing GFP-Rab13-2, REP- or PRA1-3xFLAG, and RFP or RFP-Pc12 were sampled at 1 day after a 10% ethanol treatment at 1 day-post-agroinfiltration. Total protein extracts were subjected to co-IP using anti GFP agarose beads. The precipitated proteins were immunoblotted. The level of binding was calculated as the ratio between anti-FLAG and anti-FLAG of IP by imageJ. Red asterisks indicate expected band sizes.

(D) Pc12 strengthen the weak interaction between REP and Rab13-2^{Q74L}. The plants were infiltrated with an agrobacterium carrying REP-3xFLAG and an agrobacterium containing two plasmids, one plasmid with RFP or RFP-Pc12 and the other with GFP-Rab13-2^{Q74L} or Rab13-2^{S29N}, in a 1:1 ratio in *N. benthamiana*. Samples treated with 10% ethanol at 1 dpi were collected at 12 hours post treatment. The level of binding was calculated as the ratio between anti-FLAG and anti-FLAG of IP by imageJ. Red asterisks indicate expected RFP and RFP-Pc12 band sizes.

(E) Altered localization of Rab13-2 mutants by the co-expression of RFP-Pc12. Cytosolic diffusion of GFP-Rab13-2^{Q74L} was altered to show punctate localization frequently (yellow arrows), while Golgi localization of GFP-Rab13-2^{S29N} were inhibited by the co-expression of Pc12 (white arrowheads). The brightness of the original micrograms was enhanced to improve the visibility of subcellular compartments. More than 60 z-images in 0.3 μm step size were superimposed by a maximum z-projection function in ImageJ. This processing does not change the conclusion drawn from the images. GFP was pseudo-colored to green, while RFP displayed in magenta. More than 12 images were acquired from 3 independent experiments. Scale bars, 20 μm.

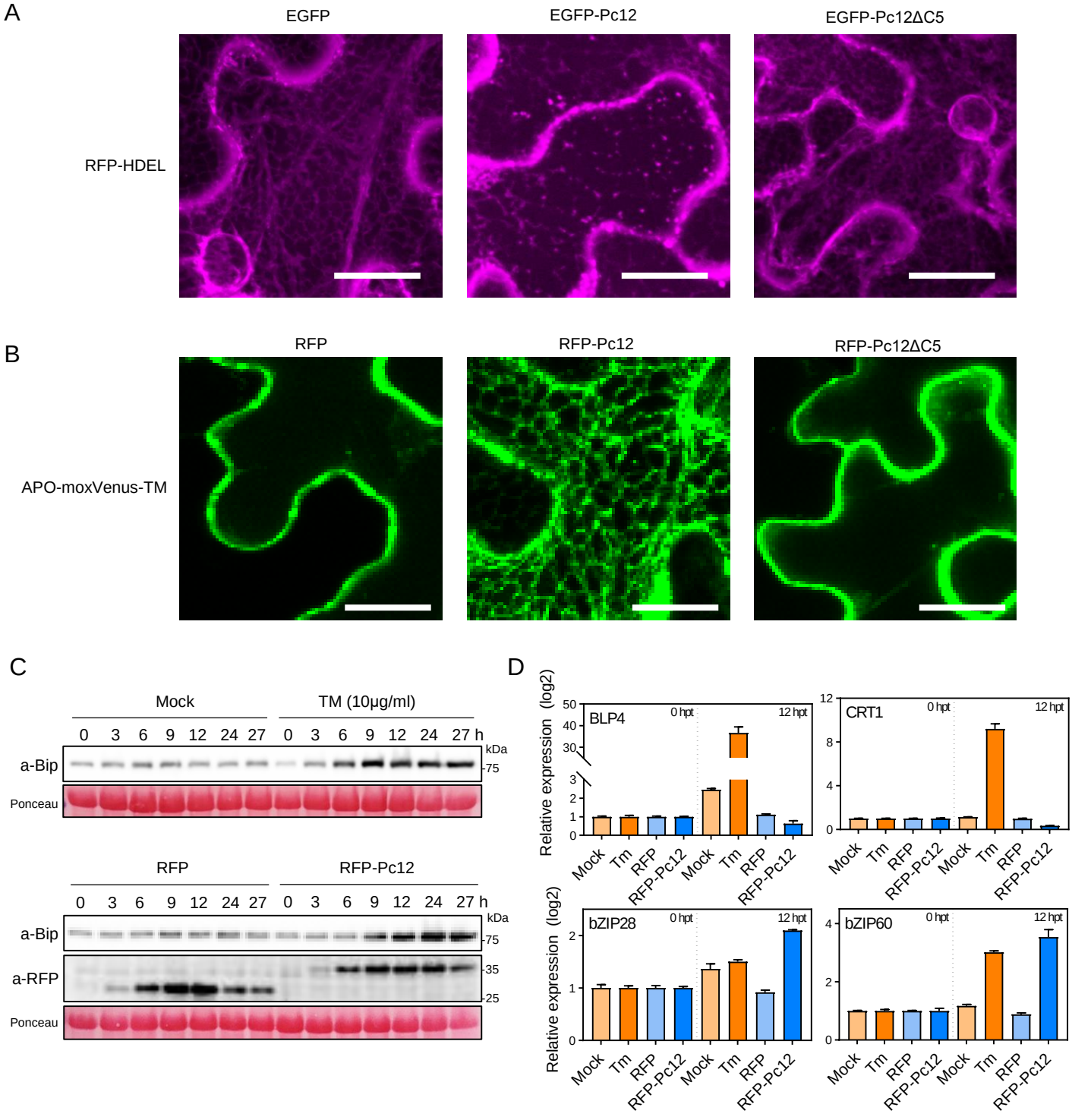
A
EGFP
EGFP-Pc12
EGFP-Pc12ΔC5
RFP-HDEL
B
RFP
RFP-Pc12
RFP-Pc12ΔC5
APO-moxVenus-TM
C
Mock
TM (10μg/ml)
0 3 6 9 12 24 27 0 3 6 9 12 24 27 h
kDa
a-Bip
75
Ponceau
RFP
RFP-Pc12
0 3 6 9 12 24 27 0 3 6 9 12 24 27 h
kDa
a-Bip
75
a-RFP
35
25
Ponceau
D
Relative expression (log2)
BLP4
0 hpt
12 hpt
CRT1
bZIP28
bZIP60
Mock
Tm
RFP
RFP-Pc12

Figure 5.

Figure 5. Pc12 inhibits the location of ER-resident RFP and the secretion of apoplastic membrane-anchored moxVenus, triggering ER stress separate from the effects of tunicamycin.
(A) Discontinuity and puncta localization of RFP-HDEL under the expression of Pc12. GFP, GFP-Pc12 and GFP-Pc12ΔC5 were transiently expressed in transgenic *N. benthamiana* expressing RFP-HDEL. More than 60 z-images in 0.3 μm step size were acquired by a spinning disc confocal microscope. Images were superimposed by a maximum z-projection function in ImageJ. The brightness of the original micrograms was enhanced to improve the visibility of subcellular compartments. This processing does not change the conclusion drawn from the images. RFP displayed in magenta. More than 12 images were acquired from 3 independent experiments. Scale bars, 20 μm.
(B) Apoplastic membrane targeted moxVenus (apoSP-moxVenus-TM) remained in ER in the existence of Pc12. RFP-Pc12, RFP- Pc12ΔC5, and RFP driven by the ethanol promoter were induced by 10% ethanol treatment. Pc12 expression inhibited the secretion of the marker proteins resulted in their accumulation in the ER. Z-images for thicker than 3 μm sections in 0.75 μm step size were acquired by a laser scanning confocal microscope. Images of the corresponding sections were processed to improve the brightness for the clarity. This processing does not change the conclusion drawn from the images. moxVenus was pseudo-colored to green. More than 12 images were acquired from 3 independent experiments. Scale bars, 20 μm.
(C) Accumulation of the ER stress marker protein (Bip) in response to Pc12 expression. Plants were treated with mock and Tm (10 ug/ml) and sampled over time. Plants expressing RFP and RFP-Pc12 after 5% ethanol treatment were sampled over time.
(D) Transcripts level of UPR-related transcription factor and ER chaperon genes upon expression of Pc12. In (C), total RNA was extracted at 0 and 12 hours after tunicamycin or ethanol treatment. UPR-related genes, ER chaperon genes (*BLP4* and *CRT1*) and transcription factor genes (*bZIP28* and *bZIP60*), were normalized with *NbEF1a* in qRT-PCR.

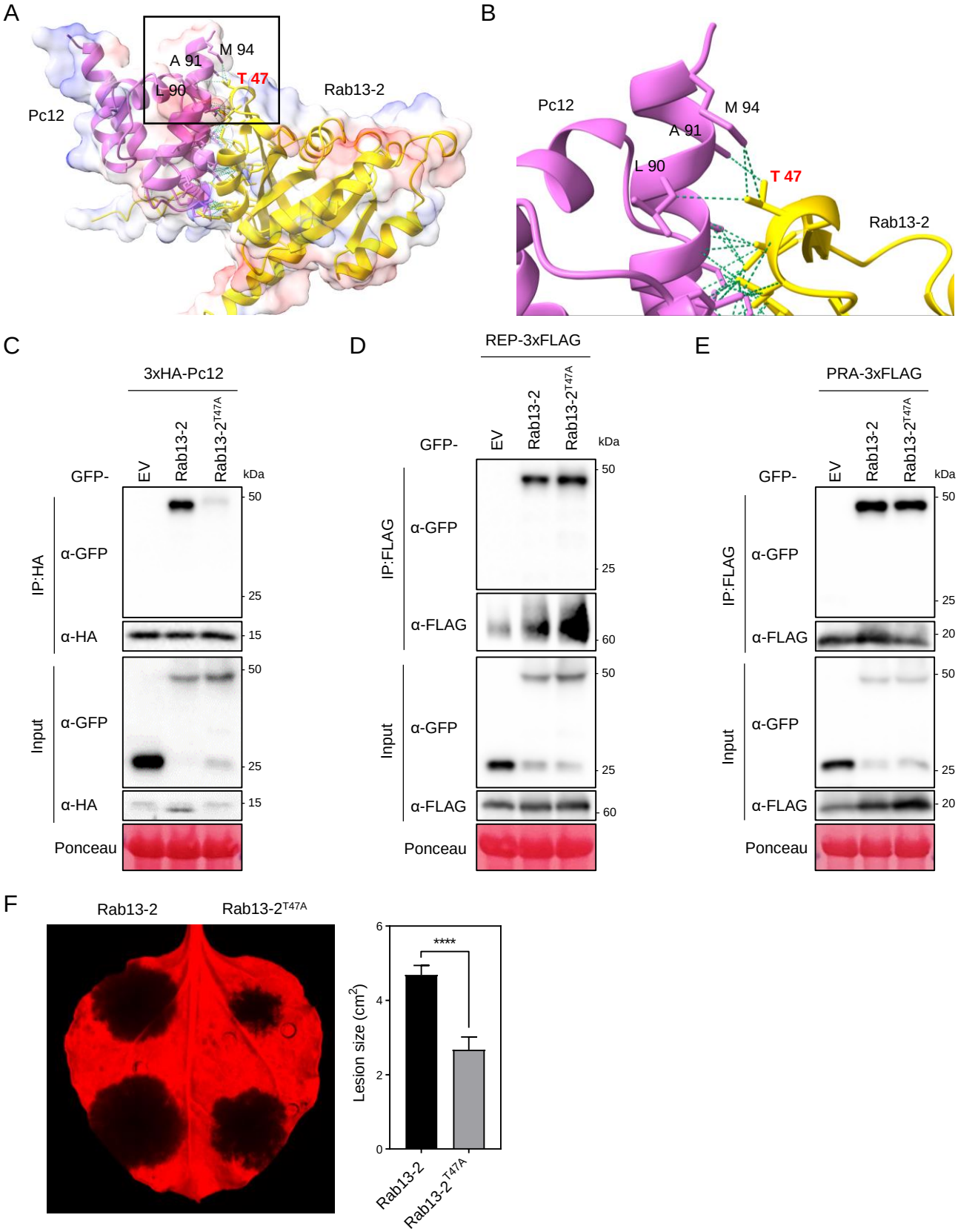
A
M 94
A 91
T 47
L 90
Pc12
Rab13-2
B
Pc12
M 94
A 91
L 90
T 47
Rab13-2
C
3xHA-Pc12
GFP-
EV
Rab13-2
Rab13-2T47A
kDa
IP:HA
α-GFP
α-HA
Input
α-GFP
α-HA
Ponceau
50
25
15
D
REP-3xFLAG
GFP-
EV
Rab13-2
Rab13-2T47A
kDa
IP:FLAG
α-GFP
α-FLAG
Input
α-GFP
α-FLAG
Ponceau
50
25
60
E
PRA-3xFLAG
GFP-
EV
Rab13-2
Rab13-2T47A
kDa
IP:FLAG
α-GFP
α-FLAG
Input
α-GFP
α-FLAG
Ponceau
50
25
20
F
Rab13-2
Rab13-2T47A
Lesion size (cm2)
****
Rab13-2
Rab13-2T47A

Figure 6

Figure 6 A mutation in a key Rab13-2 residue weakens Pc12 binding without affecting REP and PRA1 binding, compromising *P. capsici* virulence.

(A-B) The predicted structures of Pc12 and Rab13-2 interaction by AlphaFold2. (B) zooms in on the black box in (A). The green lines depict the intracellular bonds between Pc12 and Rab13-2.

(C - E) *In planta*, a co-immunoprecipitation assay with Rab13-2, Rab13-2^{T47A}, and Pc12 (REP or PRA1). Total protein extracts were precipitated with anti HA magnetic beads or anti FLAG agarose. The precipitated protein and total protein were detected by western blotting.

(F) *P. capsici* inoculation on the leaves expressing GFP-Rab13-2 and GFP-Rab13-2^{T47A}. Agrobacterium carrying GFP-Rab13-2 and GFP-Rab13-2^{T47A} was infiltrated in *N. benthamiana,* followed by *P. capsici* inoculation at 1 dpi. Images were taken at 72 hpi, and the lesion size was measured by ImageJ (N = 31 - 32, 3 repeats).

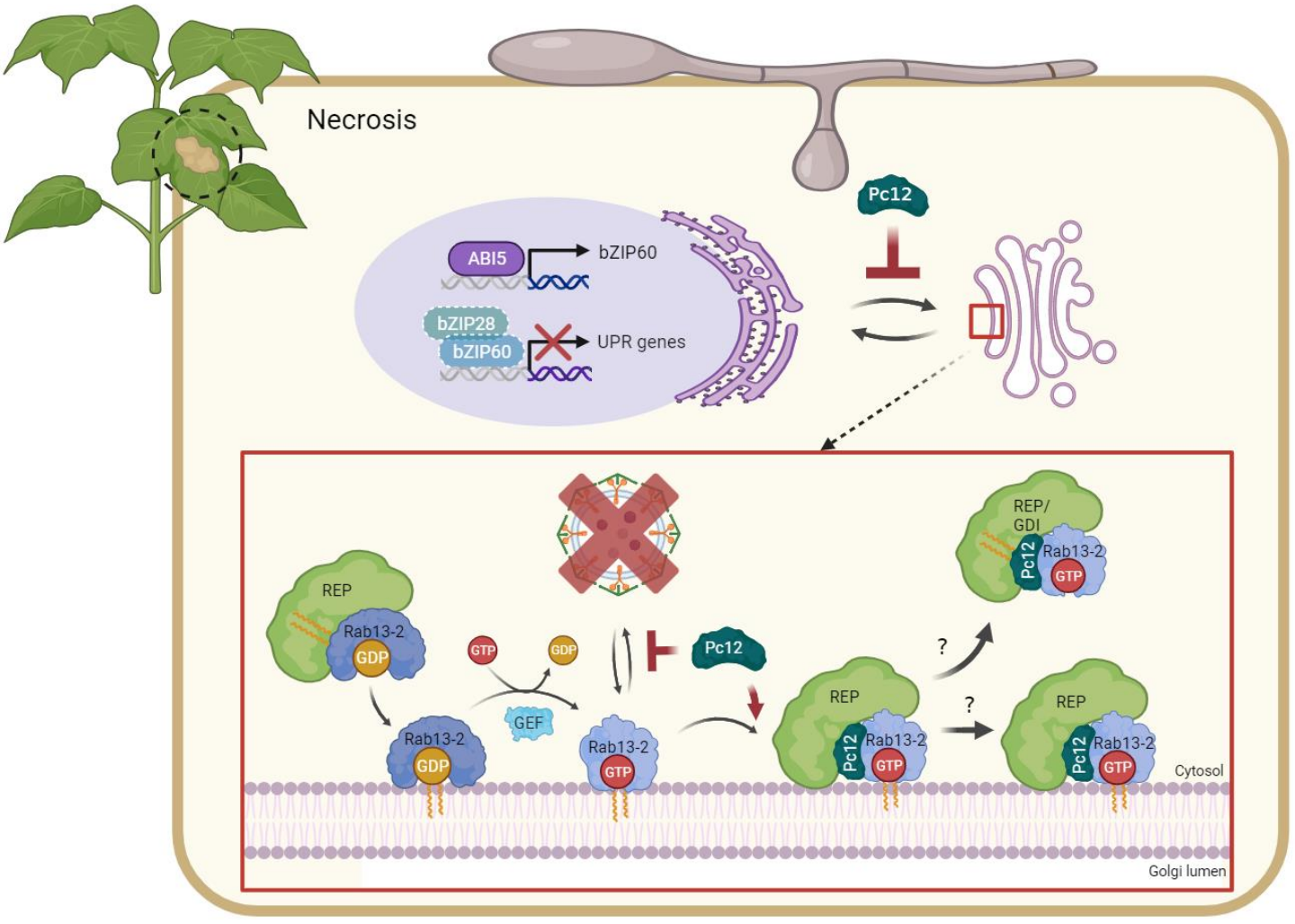

Figure 7. Summary model of the inhibition of Pc12 in Rab13-2-mediated vesicle trafficking.
Prenylated Rab13-2 in its GDP-bound state is inserted to a membrane by Rab escort protein (REP). The guanine nucleotide exchange factor (GEF) exchanges GDP for GTP on Rab13-2 to initiate vesicle formation for vesicle trafficking. Pc12, secreted from *P. capsici*, binds to GTP-bound Rab13-2, subsequently recruiting REP to facilitate the extraction of the complex from the membrane or its retention on the membrane, consequently impeding vesicle formation mediated by Rab13-2. Figure was created using BioRender.com.